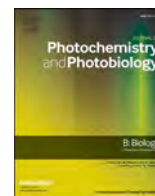




Contents lists available at ScienceDirect

Journal of Photochemistry & Photobiology, B: Biology

journal homepage: www.elsevier.com/locate/jphotobiol

Metallated phthalocyanines and their hydrophilic derivatives for multi-targeted oncological photodynamic therapy

Lionel Mendes Dias^{a,b,c,d}, Mark J. de Keijzer^{a,e,f,1}, Daniël Ernst^{a,d,1}, Farangis Sharifi^{c,g,1}, Daniel J. de Klerk^{a,d}, Tony G. Kleijn^{a,d,h}, Emilie Desclos^{c,g}, Jakub A. Kochan^{c,g}, Lianne R. de Haan^{a,d}, Leonardo P. Franchiⁱ, Albert C. van Wijk^j, Enzo M. Scutigliani^{c,g}, Marcel H. Fens^e, Arjan D. Barendrecht^k, José E.B. Cavaco^b, Xuan Huang^a, Ying Xu^l, Weiwei Pan^l, Marjo J. den Broeder^m, Jan Bogerd^m, Rüdiger W. Schulz^m, Kitty C. Castricumⁿ, Victor L. Thijssenⁿ, Shuqun Cheng^o, Baoyue Ding^{a,**,2}, Przemek M. Krawczyk^{c,g,2}, Michal Heger^{a,d,e,f,*,2}, on behalf of the Photodynamic Therapy Study Group

^a Jiaxing Key Laboratory for Photonanomedicine and Experimental Therapeutics, Department of Pharmaceutics, College of Medicine, Jiaxing University, Jiaxing, Zhejiang, PR China

^b CICS-UBI, Health Sciences Research Center, University of Beira Interior, Covilhã, Portugal

^c Department of Medical Biology, Cancer Center Amsterdam, Amsterdam UMC Location Academic Medical Center, Amsterdam, the Netherlands

^d Laboratory of Experimental Oncology, Department of Pathology, Erasmus MC, Rotterdam, the Netherlands

^e Department of Pharmaceutics, Utrecht Institute for Pharmaceutical Sciences, Utrecht University, Utrecht, the Netherlands

^f Membrane Biochemistry and Biophysics, Department of Chemistry, Faculty of Science, Utrecht University, Utrecht, the Netherlands

^g Laboratory of Experimental Oncology and Radiobiology (LEXOR), Cancer Center Amsterdam, Amsterdam UMC Location Academic Medical Center, Amsterdam, the Netherlands

^h Department of Pathology and Medical Biology, University Medical Center Groningen, University of Groningen, Groningen, the Netherlands

ⁱ Department of Biochemistry and Molecular Biology, Institute of Biological Sciences (ICB 2), Federal University of Goiás (UFG), Goiânia, Goiás, Brazil

^j Department of Surgery, Amsterdam UMC location VUmc, Amsterdam, the Netherlands

^k CDL Research, University Medical Center Utrecht, Utrecht, the Netherlands

^l Department of Cell Biology, College of Medicine, Jiaxing University, Jiaxing, PR China

^m Reproductive Biology Group, Division Developmental Biology, Institute of Biodynamics and Biocomplexity, Department of Biology, Faculty of Science, Utrecht University, the Netherlands

ⁿ Department of Radiation Oncology, Cancer Center Amsterdam, Amsterdam UMC Location VUmc, Amsterdam, the Netherlands

^o Department of Hepatic Surgery VI, The Eastern Hepatobiliary Surgery Hospital, The Second Military Medical University, Shanghai, PR China

ARTICLE INFO

Keywords:

Photonanomedicine
 Interstitially targeted liposomes
 In vitro pharmacokinetics
 Mode of cell death
 Toxicity
 Skin phototoxicity
 Pharmacodynamics
 Therapeutic efficacy
 Mouse xenograft tumor model

ABSTRACT

Background and aim: A photosensitizer (PS) delivery and comprehensive tumor targeting platform was developed that is centered on the photosensitization of key pharmacological targets in solid tumors (cancer cells, tumor vascular endothelium, and cellular and non-cellular components of the tumor microenvironment) before photodynamic therapy (PDT). Interstitially targeted liposomes (ITLs) encapsulating zinc phthalocyanine (ZnPC) and aluminum phthalocyanine (AIPC) were formulated for passive targeting of the tumor microenvironment. In previous work it was established that the PEGylated ITLs were taken up by cultured cholangiocarcinoma cells. The aim of this study was to verify previous results in cancer cells and to determine whether the ITLs can also be used to photosensitize cells in the tumor microenvironment and vasculature. Following positive results, rudimentary in vitro and in vivo experiments were performed with ZnPC-ITLs and AIPC-ITLs as well as their water-soluble tetrasulfonated derivatives (ZnPCS4 and AIPCS4) to assemble a research dossier and bring this platform closer to clinical transition.

* Corresponding author at: Jiaxing Key Laboratory for Photonanomedicine and Experimental Therapeutics, Department of Pharmaceutics, College of Medicine, Jiaxing University, Jiaxing, Zhejiang, PR China.

** Corresponding author.

E-mail addresses: lina_310@163.com (B. Ding), m.heger@jctres.com, m.heger@uu.nl (M. Heger).

¹ Shared second authorship.

² Shared senior authorship.

<https://doi.org/10.1016/j.jphotobiol.2022.112500>

Received 10 March 2022; Received in revised form 27 April 2022; Accepted 11 June 2022

Available online 17 June 2022

1011-1344/© 2022 The Authors. Published by Elsevier B.V. This is an open access article under the CC BY license (<http://creativecommons.org/licenses/by/4.0/>).

Methods: Flow cytometry and confocal microscopy were employed to determine ITL uptake and PS distribution in cholangiocarcinoma (SK-ChA-1) cells, endothelial cells (HUVECs), fibroblasts (NIH-3T3), and macrophages (RAW 264.7). Uptake of ITLs by endothelial cells was verified under flow conditions in a flow chamber. Dark toxicity and PDT efficacy were determined by cell viability assays, while the mode of cell death and cell cycle arrest were assayed by flow cytometry. In vivo systemic toxicity was assessed in zebrafish and chicken embryos, whereas skin phototoxicity was determined in BALB/c nude mice. A PDT efficacy pilot was conducted in BALB/c nude mice bearing human triple-negative breast cancer (MDA-MB-231) xenografts.

Results: The key findings were that (1) photodynamically active PSs (i.e., all except ZnPCS4) were able to effectively photosensitize cancer cells and non-cancerous cells; (2) following PDT, photodynamically active PSs were highly toxic-to-potent as per anti-cancer compound classification; (3) the photodynamically active PSs did not elicit notable systemic toxicity in zebrafish and chicken embryos; (4) ITL-delivered ZnPC and ZnPCS4 were associated with skin phototoxicity, while the aluminum-containing PSs did not exert detectable skin phototoxicity; and (5) ITL-delivered ZnPC and AIPC were equally effective in their tumor-killing capacity in human tumor breast cancer xenografts and superior to other non-phthalocyanine PSs when appraised on a per mole administered dose basis.

Conclusions: AIPC(S4) are the safest and most effective PSs to integrate into the comprehensive tumor targeting and PS delivery platform. Pending further in vivo validation, these third-generation PSs may be used for multi-compartmental tumor photosensitization.

1. Introduction

Photodynamic therapy (PDT) is a non-to-minimally invasive light-based modality for the treatment of a variety of diseases such as psoriasis, age-related macular degeneration, and cancer. The cancer types that have been clinically addressed by PDT include skin-, lung-, brain-, ovarian-, bladder-, prostate-, liver-, bile duct-, pancreatic-, esophageal-, and head and neck cancer [1]. PDT is doubly selective towards the tumor mass owing to the preponderant photosensitization of the tumor relative to surrounding healthy tissue and the confinement of illumination to the tumor bulk. The therapeutic efficacy of oncological PDT emanates from the induction of tumor cell death, damage to the tumor microenvironment, metabolic catastrophe in tumor cells due to hypoxia and malnutrition following vascular shutdown, and activation of an anti-tumor immune response with potential abscopal effects [2–5]. Notwithstanding the fact that the modality is generally used as a last-line treatment option, the abovementioned effects have rendered PDT superior to second-line treatment options such as chemotherapy and radiotherapy in terms of select clinical outcome parameters for certain cancers [6–11]. Nonetheless, several factors have deterred widespread clinical adoption of PDT, which comprise skin phototoxicity [12], the activation of tumor cell survival signaling following PDT [2,13–16] and consequent tumor regrowth or recurrence [17,18], the inability to treat large tumors due to the limited optical penetration depth of laser light and heterogeneous photon coverage of target tissue [19], and the requirement for specialized clinical teams and long post-treatment dark periods for patients [20]. The latter is ethically problematic in case of aggressive terminal cancer with short median life expectancy [21].

To counter these clinical bottlenecks our group has developed a comprehensive tumor photosensitization strategy [20,21] based on three distinct liposomal photosensitizer (PS) delivery systems that target pharmacologically critical locations in the tumor, namely the tumor cells [22], the tumor interstitial space [13,23], and the intratumoral vasculature [2,24]. Photosensitizer encapsulation into liposomes will sterically hinder extravasation of PS molecules through the fenestrations in the dermal microcirculation, thereby ameliorating PS accumulation in the skin and the incidence of phototoxic reactions [25,26]. Consequently, the circulatory confinement of PS molecules will translate to effective therapeutic outcomes at lower PS dosage. Both will concurrently reduce the required post-treatment dark periods, making the treatment more patient-friendly. By photosensitizing and oxidatively damaging distinct structural elements of the tumor, the ability of sublethally afflicted tumor cells to recover from photo-induced hyperoxidative stress will be impaired. This comprehensive photosensitization strategy therefore also tackles potential tumor regrowth or recurrence. To further offset tumor cell survival in predominantly distal tumor

regions [2], our group has developed fourth-generation photosensitizers that encompass the co-encapsulation of small-molecular drugs into PS-carrying liposomes so as to curtail post-PDT survival. Proof-of-concept with the hypoxic cytotoxin tirapazamine and the HIF-1 α and topoisomerase II inhibitor acriflavine has been established [14,15,27].

The most basic formulation of the PS delivery platform concerns interstitially targeted liposomes (ITLs) composed of dipalmitoylphosphatidylcholine and a molar fraction of PEG-conjugated distearylphosphatidylethanolamine. ITLs were designed to target the tumor stroma [28] by virtue of the enhanced permeability and retention (EPR) effect exhibited by many solid tumors [29,30] - a phenomenon exploited by several approved liposomal chemotherapeutic carriers [31–35]. The tumor microenvironment is an established target for cancer treatment, including PDT [3]. In previous studies it was demonstrated that PS-encapsulating ITLs, which do not bear targeting moieties or possess uptake-enhancing properties, were endocytosed by cultured biliary cancer (SK-ChA-1) [13,23] and skin cancer (A431) cells [21], thereby fundamentally enabling multi-targeting. It was further shown that, upon illumination, the metallated phthalocyanine-containing ITLs produced reactive transients capable of oxidizing (bio) molecules [20,23,36], culminating mainly in apoptotic and necrotic cell death at half maximum lethal concentration (LC₅₀) values in the low-nM range for both zinc phthalocyanine (ZnPC) and aluminum phthalocyanine (AIPC) and their hydrophilic tetrasulfonated derivatives ZnPCS4 and AIPCS4 [13,21,23].

In light of the abovementioned properties, the non-toxicity of the formulation in chicken embryos and mice [13], and the GMP scaling possibilities it was decided to further develop the formulation in the context of extrahepatic cholangiocarcinoma (EHCC). Presently, non-resectable EHCC (~80% of patients [37]) is incurable and responds poorly to standard and palliative chemotherapy [38]. Accordingly, there is a strong medical need to develop effective therapies for EHCC. PDT constitutes a promising last-line therapy for EHCC, as corroborated in numerous clinical trials [17,39–42]. EHCCs have a major stromal component that is replete with neoangiogenic vasculature [14], rendering these tumors eligible for ITL-based photosensitization.

This study therefore aimed to validate previous results obtained with abovementioned PSs in SK-ChA-1 [23] and A431 cells [21] in cells that are instrumental in tumor biology and comprise key elements in our comprehensive tumor targeting strategy: SK-ChA-1 cells that are representative of the tumor parenchyma [43], RAW 264.7 cells that mimic tumor-resident macrophages [44], NIH-3T3 cells as substitutes for stromal fibroblasts [45], and human umbilical vein endothelial cells (HUVECs) that are analogous to the endothelial cells lining the intratumoral microvasculature [14]. ITLs encapsulating ZnPC and AIPC as well as non-encapsulated ZnPCS4 and AIPCS4 were assayed for uptake,

intracellular localization, dark toxicity, photodynamic efficacy, and PDT-induced mode of cell death and cell cycle arrest. Given the encouraging *in vitro* data, the ITLs were screened for systemic toxicity in zebrafish and chicken embryos and for skin phototoxicity in nude mice. Finally, an *in vivo* pharmacodynamic efficacy pilot study was conducted with the liposomal PSs in mice bearing human triple-negative mammary carcinoma (MDA-MB-231) xenografts.

2. Materials and Methods

Supplemental material is designated with prefix 'S' and the section numbering in the supplemental material corresponds to that in the main text. A list of abbreviations is provided in the supplemental material. The chemicals/compounds, buffers, and reagents/kits are summarized in Table S1. Equipment and materials/disposables are listed in Table S2. Cells and animals and their required paraphernalia are summarized in Table S3. The concentrations listed are final unless specified otherwise. All procedures involving PSs were performed under dim light.

2.1. Photosensitizers, Phospholipids, and Buffers

ZnPC and AlPC were dissolved in pyridine at a 178- μ M and 150- μ M stock concentration, respectively. ZnPCS4 and AlPCS4 were dissolved in phosphate-buffered saline (PBS) at a 1-mM stock concentration. All PS stock solutions were stored under a nitrogen atmosphere at room temperature (RT) (ZnPC and AlPC) or 4 °C (ZnPCS4 and AlPCS4) in the dark.

Phospholipids (Table S1) were dissolved in chloroform and stored under a nitrogen atmosphere at -20 °C. The phospholipid concentration of stock solutions was determined spectrophotometrically by an inorganic phosphate quantification method modified from Rouser et al. [23,46].

Physiological buffer was composed of 10 mM HEPES, 0.88% (w/v) NaCl, pH=7.4 that was attuned to physiological conditions (0.293 osmol/kg) [23].

2.2. Cell Culture

2.2.1. Cell Culture for *In Vitro* Experiments

HUVECs were isolated from fresh umbilical cords obtained at the Department of Obstetrics and Gynecology of the Academic Medical Center (Amsterdam University Medical Centers) and processed as described previously [47]. SK-ChA-1 cells were obtained from malignant ascites of a patient with primary adenocarcinoma of the extrahepatic biliary tree [43]. Cell and cell line details are provided in section S2 (Table S3). Cells were grown under standard culture conditions (dark, 37 °C, humidified atmosphere composed of 5% CO₂ and 95% air). Readers are referred to section S2.2 for cell culture details.

The cells were washed with PBS (RT, 10 mL/T75 flask) prior to detachment by Accutase treatment (1 mL/T75 flask) for 10 min under standard culture conditions or by using a cell scraper in the case of RAW 264.7 macrophages (to prevent cell activation). Cells were harvested by the addition of fully supplemented culture medium and transferred to a new T75 flask.

Cells, detached as described above, were seeded into 24-well plates 24 h prior to an experiment unless stated otherwise. The seeding density (section S2.2) was such that ~90% confluence was reached at the time of the experiment. Cell counting was performed with an aliquot of 10 μ L using a hemocytometer and a brightfield microscope.

During the experiments, medium without fetal bovine serum (FBS) and phenol red (medium^{-/-}) was used when cells were incubated with PSs or reagents.

2.2.2. Cell Culture for *In Vivo* Experiments

Human triple-negative breast cancer (MDA-MB-231) cells were grown in T25 culture flasks under standard culture conditions in RPMI 1640 (further detailed in section S2 (Table S3)). The medium was

supplemented with 10% FBS, 100 μ g/mL streptomycin, and 100 U/mL penicillin. The cells were washed once with PBS (RT) and detached by trypsin (1 mL per T25 flask, 2 min). Cells were resuspended in cell culture medium and centrifuged at 100 \times g for 15 min at RT. The cell pellet was resuspended in cell culture medium at 3×10^6 cells/mL and Matrigel at a 1:1 ratio. The mixture was kept on ice until subcutaneous injection into the right dorsal flank of the animal (see further Section 2.14.2).

2.3. Preparation, Characterization, and Functional Testing of ITLs

2.3.1. Preparation

ITLs composed of 1,2-dipalmitoyl-*sn*-glycero-3-phosphocholine (DPPC) and L- α -phosphatidylethanolamine, distearoyl methoxypolyethylene glycol conjugate (DSPE-PEG) (96:4 molar ratio) were prepared by the lipid film hydration technique as described previously [23]. Briefly, the phospholipids and ZnPC or AlPC were premixed at the desired ratios and the organic phase was evaporated under a stream of nitrogen gas at 40 °C in a water bath. The lipid film was vacuum exsiccated for 30 min and hydrated with physiological buffer (Section 2.1). The suspension was tip sonicated and the liposomes were stored at 4 °C under a nitrogen atmosphere in the dark for a maximum of 2 months [15]. The PS:phospholipid molar ratio was 0.003 [21,23].

Where indicated, fluorescently labeled ITLs were prepared by the incorporation of 1,2-dipalmitoyl-*sn*-glycero-3-phosphoethanolamine-N-(lissamine rhodamine B sulfonyl) (rhodamine-PE, headgroup-labeled) and/or 1-palmitoyl-2-(6-[(7-nitro-2-1,3-benzoxadiazol-4-yl)amino]hexanoyl)-*sn*-glycero-3-phosphocholine (NBD-PC, acyl chain-labeled) into the lipid bilayer at the expense of DPPC. Rhodamine-PE was incorporated at a 1.0% molar fraction while NBD-PC was included at a 5.0% molar fraction.

The ITLs that were used in the chicken embryo toxicity studies were prepared at a 20-mM phospholipid concentration and a 0.003 PS: phospholipid molar ratio. Instead of physiological buffer, 0.75% (w/v) NaCl in sterile MilliQ was used as lipid film hydration solution. ZnPCS4 and AlPCS4 were dissolved in PBS at a 3-mM stock concentration and diluted with MilliQ to arrive at a final concentration of 2.56 mM and to ensure iso-osmolality relative to chicken embryo blood.

2.3.2. Characterization

Liposomes were characterized for size and polydispersity as well as zeta-potential by dynamic light scattering and electrophoretic mobility analysis, respectively, as described in [21,23]. The mean \pm SD size [range] of ZnPC-ITLs and AlPC-ITLs used in the experiments was 120 ± 8 nm [109–127 nm] and 175 ± 10 nm [162–189 nm], respectively, with a mean \pm SD polydispersity index of 0.374 ± 0.133 and 0.612 ± 0.098 . The mean \pm SD size [range] zeta-potential was -6.3 ± 5.4 [-2.3 to -10.1] for ZnPC-ITLs and -7.6 ± 4.5 [-3.2 to -9.6] for AlPC-ITLs.

2.3.3. Functional testing

Functional testing was performed by a protein oxidation assay as described earlier [23] and as detailed in section S2.3.3. Bovine serum albumin (BSA) was used as a model protein to assess whether PDT-induced ROS was able to induce protein oxidation. BSA contains tryptophan which autofluoresces when excited at 279 nm. Oxidation of tryptophan abrogates its intrinsic fluorescence properties. A reduction in tryptophan fluorescence was therefore used as an outcome parameter for protein oxidation.

2.4. Temperature-Dependent Uptake of ITLs (Flow Cytometry)

The effect of temperature on ITL association was investigated by incubation of cells with rhodamine-PE-labeled ITLs (Section 2.3) at 4 °C and 37 °C. A solution containing ITLs in medium^{-/-} was prepared at 50, 100, and 250 μ M final phospholipid concentration. The upper

concentration limit was selected because roughly 5% of injected PEGylated lecithin liposomes passively target to the tumor following 24 h of circulation in mice [48] and PEGylated lecithin liposomes are typically administered at a systemic phospholipid concentration range of 0.02–3.3 mM in mice [49]. ITLs were added to cells cultured in 12-well plates to ~90% confluence and incubated for 2 h under normoatmospheric conditions at 4 °C (refrigerator) and 37 °C (stove). Next, cells were washed with PBS (1 mL/well) and harvested using 50 μ L/well of Accutase for 10 min at standard culture conditions or by scraping (RAW 264.7 cells). Harvested cells were collected in 500 μ L medium^{-/-}, transferred to 2-mL centrifuge tubes, and kept on ice until centrifugation. Following centrifugation (5 min, 200 \times g, 4 °C) the supernatant was discarded and cells were resuspended in 500 μ L of medium^{-/-} before transfer to 5-mL round-bottom polypropylene tubes for flow cytometric analysis.

Viable cells were gated based on forward scatter and side scatter properties. Rhodamine-PE fluorescence was measured at $\lambda_{\text{ex}} = 488$ nm and $\lambda_{\text{em}} = 585 \pm 42$ nm as an indicator of ITL-cell association (section S2.4). Ten thousand counts were collected in the gated region. Fluorescence intensity was averaged from 3 experimental replicates per concentration. Data were processed in FlowJo software and plotted in GraphPad Prism.

2.5. ITL Internalization and Intracellular Distribution (Confocal Microscopy)

ITL internalization and intracellular localization were studied by confocal microscopy. The cells were seeded on fibronectin-coated 24-mm circular coverslips placed in 6-well plates as described in [15,27] and grown overnight as described in section S2.2.1 until 60–70% confluence. After washing once with PBS (37 °C), ITLs labeled with NBD-PC and rhodamine-PE (Section 2.3) were added at final phospholipid concentration of 250 μ M to medium^{-/-} and incubated for 15, 30, and 60 min under standard culture conditions. Next, cells were washed and imaged as further detailed in section S2.5 and Tables S4 and S5.

2.6. Uptake of ITLs by Endothelial Cells under Flow

Rhodamine-PE-labeled ITLs were prepared and characterized as described in Section 2.3. HUVECs were purchased from Lonza and seeded in Ibidi perfusion slides at a density of 2.4×10^5 cells/slide in a total volume of 150 μ L of complete EBM-2 medium containing SupplementMix and antibiotics (GA-1000) and allowed to attach for 2 h. Subsequently, the slides were connected to a yellow/green pump-controlled perfusion set (50 cm, internal diameter 1.6 mm, 10 mL reservoirs, Ibidi) and cultured for 3 d under continuous unidirectional flow (shear rate 300 s⁻¹, shear stress 0.3 N/m² (3.0 dyn/cm²), viscosity 1 mPa \cdot s (0.01 dyn \cdot s/cm²), and pressure 9.3 mbar) using PumpControl v1.5.4 software at 37 °C and 5% CO₂ in complete EBM-2 medium.

Just before the addition of the different liposomes, the old medium was removed from the pump system and flushed with 10 mL of fresh EBM-2 medium without growth factors and serum, that was in turn removed. Subsequently, 10 mL of sample in EBM-2 medium without growth factors, antibiotics, and serum was added to the 2 mL of medium remaining in the pump system, and liposomes were added at a final lipid concentration of 150 μ M. HUVECs were incubated with the liposomes for 30 min at aforementioned unidirectional flow settings. Subsequently, the slides were disconnected and washed twice with 2.5 mL of EBM-2 medium. The cells were then fixed with 4% paraformaldehyde in PBS. After fixation, the nuclei were stained with 1 μ g/mL Hoechst 33342 in PBS for 20 min and washed once with PBS. The F-actin cytoskeleton was stained with Alexa Fluor 488 (AF488)-conjugated phalloidin (1:50 in PBS) for 30 min and washed once with PBS. Finally, the cells were mounted with FluorSave reagent. Imaging was performed using a Zeiss Axio Observer Z1 microscope and images were processed using ZEN 2 Blue software and ImageJ software as further detailed in section S2.6.

2.7. Cell Photosensitization (Flow Cytometry and Confocal Microscopy)

The relative degree of cell photosensitization was studied by flow cytometry. All four PSs were diluted in medium^{-/-} to a PS concentration of 375 nM, corresponding to a final phospholipid concentration of 125 μ M for ZnPC-ITLs and AlPC-ITLs.

PSs were added to cells cultured in 12 wells-plates to 80% confluence. The plates were incubated for 1, 30, and 60 min under standard culture conditions. After harvesting with 100 μ L of Accutase for 10 min at standard culture conditions (or scraping in the case of RAW 264.7 macrophages), cells were collected in 500 μ L of medium^{-/-} at RT, transferred to a 2-mL centrifuge tube, and centrifuged (5 min, 500 \times g, 4 °C). The supernatant was discarded and the cells were resuspended in 500 μ L of medium^{-/-} (RT) for flow cytometric analysis.

Viable cells were gated based on their preset forward scatter and side scatter properties. PS autofluorescence was measured at $\lambda_{\text{ex}} = 633$ nm and $\lambda_{\text{em}} = 661 \pm 20$ nm and a fixed detector voltage (625 V). The excitation wavelength coincides with the blue Q-band absorption shoulder of the PSs [20], and causes autofluorescence as a result of radiative S₁ -> S₀ state decay of a small fraction of the excited state electrons. Ten thousand events were collected in the gated region. Association was calculated from the difference between the mean fluorescence intensity of photosensitized cells relative to the mean fluorescence intensity of non-photosensitized cells ($N = 3$ independent experiments per incubation time). Data were processed in FlowJo software and GraphPad Prism.

After washing with PBS (37 °C), cells were incubated with 10 μ M of AlPCs4 or ZnPCS4 or 3 μ M of ZnPC or AlPC (1 mM phospholipid concentration) for 1, 30, and 60 min at standard culture conditions.

2.8. Dark Toxicity in Cultured Cells

The toxicity of each PS was assessed in SK-ChA-1, HUVEC, NIH-3T3, and RAW 264.7 cells in the absence of illumination. Cells seeded in 24-wells plates were washed with PBS at RT, and PS in medium^{-/-} was added at concentrations ranging from 0 to 1.5 μ M for ZnPC-ITLs and AlPC-ITLs (0–500 μ M phospholipid concentration, equating to 0–1.5 μ M PS concentration) and 0–10 μ M for ZnPCS4 and AlPCS4. Medium^{-/-} containing 20% DMSO was used as positive control for complete cell death and medium^{-/-} as negative control. After 24-, 48-, and 72-h incubation at standard culture conditions, WST-1 and SRB assays were performed in sequence on the same cell population as described previously [21] and detailed in section S2.8. Experiments in each group (PS concentration and incubation time) were performed in triplicate.

2.9. PDT of Cultured Cells

To compare photodynamic efficacy between the PSs, mitochondrial redox state and total protein content were measured after PDT. Cells seeded in 24-wells plates were incubated for 1 h with PS in medium^{-/-} under standard culture conditions. The volume of physiological buffer containing the PS (50 μ L added to 450 μ L medium^{-/-}) was kept constant while initial PS concentration was controlled via dilution with physiological buffer. Following photosensitization, cells were washed once with PBS (RT, 500 μ L/well) and received fresh medium^{-/-} (37 °C, 500 μ L/well). The cells were illuminated with a 671-nm solid state diode laser at 500 mW for 57 s/well (the diameter of the beam was equal to the diameter of a well), yielding a cumulative radiant exposure of 15 J/cm². The laser output power was confirmed with a power meter before PDT. The plate was kept at 37 °C using a plate heater during PDT. Following illumination, the cells were incubated in medium^{-/-} for 4 h or 24 h ($N = 3$ independent experiments per time point and PS concentration) under standard culture conditions to emulate PDT-induced malnutrition due to vascular shutdown [50,51]. Lastly, the WST-1 assay and subsequent SRB assay were performed as described in sections S2.8.1 and S2.8.2, respectively. The results were normalized to the mean of the

control group that had been illuminated but not photosensitized. LC_{50} values were obtained using the non-linear fit function in GraphPad Prism.

2.10. Cell Cycle Analysis

To determine the effect of PDT on the cell cycle, PDT-treated cells were stained with propidium iodide (PI) and analyzed by flow cytometry [14,15,27]. PDT was performed on photosensitized cells in medium^{-/-}, illumination for 1 min and 54 s at 500 mW (cumulative radiant exposure of 15 J/cm² per well), with $N = 3$ independent experiments per PS. The percentage of the cell population in the G_0/G_1 phase, S phase, and G_2/M phase was calculated using the Watson (Pragmatic) univariate model [52] in FlowJo software. Additional details are provided in section S10.

2.11. Analysis of Mode of Cell Death

The mode of cell death was analyzed by flow cytometry. Cells were photosensitized and treated by PDT as described in Section 2.10 and analyzed at 2 h, 4 h, and 8 h post-PDT ($N = 3$ independent experiments per time point). The experiment was repeated for the 4-h post-PDT incubation group, where the PS concentration effects were studied. Viable cells were quantified as AV-negative / PI-negative, while cells that were in early apoptosis were quantified as AV-positive / PI-negative. Cells in late apoptosis and necrosis were clustered and quantified as AV-positive / PI-positive and AV-negative / PI-positive, respectively (modified from [53]). Data were plotted in GraphPad Prism. More information on experimental detail is provided in section S11.

2.12. Systemic Toxicity in Zebrafish Embryos

Wild-type, AB strain, *Danio rerio* adults were bred and raised in the aquatic facility of the Faculty of Science, Utrecht University. Institutional review board approval regarding the zebrafish experiments was exempted inasmuch as the embryos were in a non-vertebrate stage (≤ 5 days post-fertilization (dpf)) throughout the experiment and hence did not meet the animal ethics review criteria under Dutch legislation. Zebrafish care is described in section S2.12.

The fertilized eggs were collected 30 min after spawning, washed with sterile water, and transferred to E3 medium (5 mM NaCl, 0.17 mM KCl, 0.33 mM CaCl₂•2H₂O, 0.33 mM MgSO₄•7H₂O) in a 100 × 15 mm Petri dish. The fertilization rate was observed under a Nikon SMZ-800 stereomicroscope and the experiment was continued when fertilization was $>90\%$. Embryos in 4- to 32-cell stage were selected and transferred to a 96-wells plate with 100 μ L test solution comprising 95% E3 medium and 5% PS, with a final PS concentrations ranging from 0.19 to 1.5 μ M for liposomal ZnPC and AIPC (62.5–500 μ M final phospholipid concentration) and from 16.25 to 150 μ M ZnPCS4 and AIPCS4. The volume containing the PS was kept constant. One embryo was used per well, with a total of 8 embryos per PS concentration. The embryos were kept in an incubator at 28.0 ± 0.5 °C in the dark to prevent phototoxicity. Medium was refreshed every 24 h with medium containing the same concentration of PS.

Survival and hatch rate of embryos were recorded daily, and morphology and teratogenicity at 120 h post-fertilization (hpf) were scored by two researchers (DE and MJdB) as described in [54] and detailed in section S2.12. Group results were discarded when morphological effects had materialized in $>20\%$ of the control embryos. On the last day of the experiment, images were taken after anesthetizing the zebrafish embryos with 1 drop of MS222 using a Motic SMZ-171 T stereomicroscope equipped with a Moticam 5 digital camera. Images were processed with Motic Images Plus 3.0 software.

2.13. Systemic Toxicity in Chicken Embryos

In vivo toxicity was further evaluated in chicken embryos at the Department of Radiation Oncology, Cancer Center Amsterdam. In the Netherlands, chicken embryos are not considered vertebrates until embryonic development day 18 (EDD18). Approval by the animal ethics committee was therefore not required.

PSs were introduced into chicken embryos by intravenous injection as described previously [55]. Briefly, fertilized white Leghorn chicken eggs were incubated and rotated in a fan-assisted humidified incubator at a relative air humidity of 65% and a temperature of 37.8 °C for 3 d. On EDD3, a small opening of approximately 3 mm in diameter was made in the eggshell at the top of the egg and sealed with tape. The eggs were then incubated for 3 d with the opening facing upwards and without rotation. On EDD6, the small opening was enlarged to a 0.5-mm² window, sealed with tape, and the eggs were placed back in the incubator. On EDD10, 50 μ L of control or PS formulation was slowly (2–5 min) injected intravenously under a stereomicroscope using a 33-G Hamilton needle and a 100- μ L Hamilton syringe. The PS stock solutions were not further diluted (Section 2.3), yielding a systemic PS concentration of 0.8 μ M (injected dose of 1.2 nmol of ZnPC and AIPC) and 85 μ M (injected dose of 128 nmol of ZnPCS4 and AIPCS4) when a blood volume of 1.5 mL is accounted for on EDD10 [56]. Two control groups were included in this experiment, receiving 0.75% NaCl or 0.82× PBS, which are isoosmolar relative to chicken embryo blood. Following injection, eggs were placed back in the incubator and viability of the embryo was monitored daily (except for the weekend) until EDD18. At the end of the experiment, embryos were cryogenically euthanized at -20 °C for 24 h. Experiments were performed at least in duplicate and a minimum of 10 eggs were evaluated for each treatment/controls. Formulation toxicity was determined by death rate and plotted in Kaplan-Meier format as a function of EDD in GraphPad Prism.

2.14. Phototoxicity and PDT Efficacy Experiments in Mice

Mouse experiments were performed at the Jiaxing Key Laboratory for Photonanomedicine and Experimental Therapeutics of Jiaxing University's College of Medicine. All animal procedures were approved by the animal ethics and welfare committee of Jiaxing University Medical College under protocol number JUMC2019–003 (phototoxicity) and JUMC2019–059 (PDT efficacy). Animals were treated in accordance with the Guide for the Care and Use of Laboratory Animals (8th edition, National Institutes of Health, Bethesda, MD) and institutional guidelines.

2.14.1. Skin Phototoxicity in BALB/c Nude Mice

The experimental setup was custom-built and integrated into the animal housing facility infrastructure (Fig. 1).

Specific pathogen-free male BALB/c nude mice ($N = 17$) weighing between 20.5 and 23.7 g (mean \pm SD = 21.9 ± 0.9 g) on the day of PS infusion were purchased from Changzhou Cavens Laboratory Animals Co. (Changzhou, Jiangsu, China). Animal care is detailed in section S12.14.1.

On day 1, the mice were weighed and anesthetized with diethyl ether in a drying chamber (Fig. 1A). The diethyl ether was dripped on a bed of cotton placed on the bottom of the chamber. The bottom compartment was closed off with 18 cm-diameter laboratory filter paper positioned between the cotton and the hole-containing ceramic base on which the animals were placed. Anesthetic depth was confirmed by monitoring motion, breathing rate, and the response to pain stimuli (pinching of the paw). Upon reaching a desired analgesic state, the animals were transferred to a sterile surgical pad and the legs were secured to the pad with tape. The mice received a single bolus of PS (10 mM phospholipid

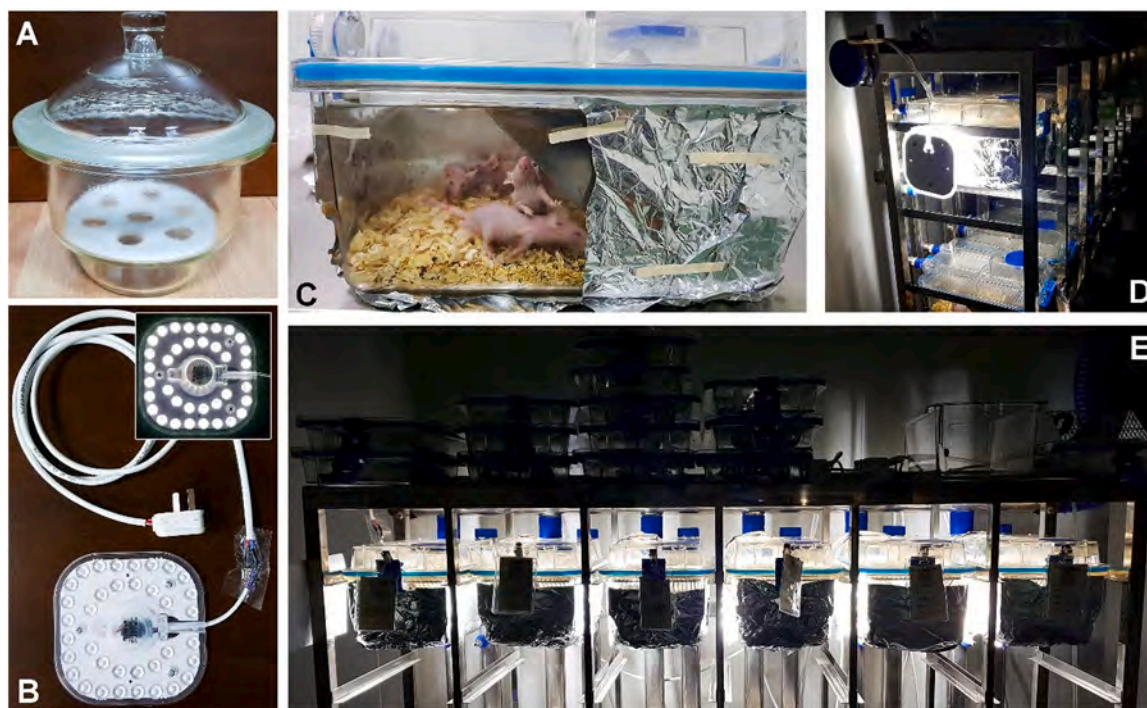


Fig. 1. Experimental setup for skin phototoxicity analysis in nude mice. (A) Anesthesia induction chamber. (B) LED panel (18 W) that was used as a source of light to emulate typical outdoor and indoor lighting conditions that photosensitized patients could be exposed to, producing an incident illuminance of 3982–5033 lx (mean \pm SD = 4558 \pm 537 lx) at the level of the animals. The insert shows the LED panel in on mode. (C) Cage setup with the created window to which the LED panel was affixed for light exposure. The sides and bottom of the cage were covered in aluminum foil. (D and E) Individual ventilated cage setup during the skin phototoxicity study, which lasted 24 h. Active climatization of the cages prevented animal exposure to hyperthermic conditions.

concentration, 0.003 PS:phospholipid molar ratio) via the penile vein (0.3 nmol/g body weight, equating to 10 μ L/g) as described in [36,57] using a 1-mL insulin syringe with a 30-G needle (Microfine, BD Biosciences). With a blood volume of 78–80 mL/kg body weight and a mean weight of 22 g, the systemic PS concentration was \sim 4 μ M. It is recommended to use insulin syringes for accurate dosing because these syringes have minimal dead volume. Group sizes were $N = 4$ (ZnPC-ITLs, ZnPCS4, AIPCS4) and $N = 5$ (AIPC-ITLs). The animals were placed back in the cage and, upon completion of a group, the side and bottom of the cage was sealed with aluminum foil to shield the photosensitized mice from light.

Twenty-four hours after PS injection (day 2), all added nesting material was removed. An 18-W LED panel (Fig. 1B) emitting white light (Fig. 1C) was used as PS excitation source to emulate outdoor and indoor lighting conditions that photosensitized patients are subjected to. The emission spectrum of sunlight and the LED panels was measured with an Ocean Optics QE65000 spectrometer. The spectrometer was connected to a modified Leica M165 FC fluorescence stereomicroscope [36] in case of LED panel measurements. The emission spectrum of the LED panel is presented against the visible light spectrum of daylight and the absorption spectrum of each PS in Fig. S4. One LED panel was fixed to the side of each cage where the aluminum foil had been removed (Fig. 1D–E). This configuration yielded an illuminance ranging from 3982 to 5033 lx (mean \pm SD = 4558 \pm 537 lx) in the center of the cage at the level of the bedding. The rest of the aluminum cover was not removed to ensure light reflection throughout the cage and to keep out stray light from neighboring cages. Mice received 125 μ L of butorphanol (1 mg/mL injection solution that was diluted 5 \times with PBS, \sim 1.3 μ g/g) subcutaneously in the dorsal neck region for analgesic purposes. Next, the LEDs were turned on for 24-h light exposure.

After 24-h illumination (day 3), the animals were terminated by cervical dislocation following diethyl ether anesthesia. Mice were inspected macroscopically for skin damage (burns, erythema, crusting, hemorrhage) and photographed (Galaxy S8, Samsung Electronics). Skin

biopsies were fixed in formalin for 6 h at RT and for 24 h at 4 $^{\circ}$ C, dehydrated in graded steps of ethanol (50%, 70%, 80%, 95%, and 100%, 1 h 2 \times /step), cleared in xylene (30 min, 2 \times), and embedded in paraffin. Five- μ m thick sections were cut with a microtome, stained with hematoxylin & eosin (H&E), and mounted on standard light microscopy slides. Three to 10 sections per mouse were assessed by two histopathologists (YX and TGK) blinded to the groups at 100, 200, and 400 \times magnification. Abnormalities such as erosions, ulceration, epidermal changes, hemorrhage, edema, influx of inflammatory cells, destruction of dermal adnexa, and fat necrosis were evaluated. The influx of inflammatory cells was scored as absent/normal (0), mild (1), and moderate (2) and the score was averaged per group.

2.14.2. In Vivo PDT Efficacy in Human Tumor-Bearing BALB/c Nude Mice

A total of 25 male BALB/c nude mice (4–6 weeks old) weighing between 19.9 and 25.3 g on the day of PS injection (day 0) were included in this pilot study and maintained as described in section S2.14.1. Mice were acclimated to laboratory conditions for 2 wk before xenografting.

MDA-MB-231 cells were cultured and injected as described in Section 2.2.3. Upon reaching a tumor volume between 100 and 200 mm³ the animals were randomly assigned to 1 of 3 groups: control ($N = 7$), ZnPC-ITLs ($N = 6$), AIPC-ITLs ($N = 7$). A total of 4 mice did not develop a tumor and 1 animal died from anesthesia.

Mice were weighed and anesthetized with diethyl ether in an anesthesia induction chamber (Fig. 1A) as described in Section 2.14.1. When a desired analgesic depth was achieved, the animals were transferred to a sterile surgical pad and the legs were secured to the pad with tape (Fig. S4A). Mice received a single bolus of ZnPC-ITLs or AIPC-ITLs (10 mM final lipid concentration, 200 μ L injection volume, 6 nmol PS per animal) or PBS (control group) via the penile vein, using a 1-mL insulin syringe with a 30-G needle, yielding a systemic PS concentration of \sim 3 μ M. A maintenance anesthesia chamber comprising diethyl ether-primed cotton balls placed in a 500-mL Erlenmeyer flask (Fig. S4B) was used when necessary to properly sedate the animals during the

injection procedure. The animals were placed back in the cage and controlled housing environment (dim light) until PDT was performed.

PDT was performed 24 h after PS administration. Mice were anesthetized as described in Section 2.14.1 and transferred to a sterile surgical pad where the animals were secured with surgical tape on their ventral side to expose the tumor region (Fig. S4C). A 671-nm solid state diode laser coupled to an optical fiber (inner diameter of 400 μm) was allowed to equilibrate for 30 min prior to PDT to ensure constant power output. The laser probe was secured in a portable retort stand and clamp and positioned approximately 3 cm from the tumor surface, accounting for an incident spot diameter of 1 cm. PDT was performed at 200 mW

output power (incident irradiance of 255 mW/cm^2), confirmed with a power meter before illumination, for 13 min and 6 s to yield a cumulative radiant exposure of 200 J/cm^2 .

Following PDT, the animals were returned to their cage and light-controlled environment. Mice were inspected macroscopically for skin damage and general wellbeing every day during 20 d post-administration. The animals were weighed every 2 d and tumor length (L) and width (W) were measured with a digital Vernier caliper. Tumor volume (V) was calculated by $V = 0.5 [L^2 \times W]$ [58]. A tumor volume of 1800 mm^3 was set as human endpoint, the reaching of which resulted in the sacrifice of the diethyl ether-anesthetized mice by cervical

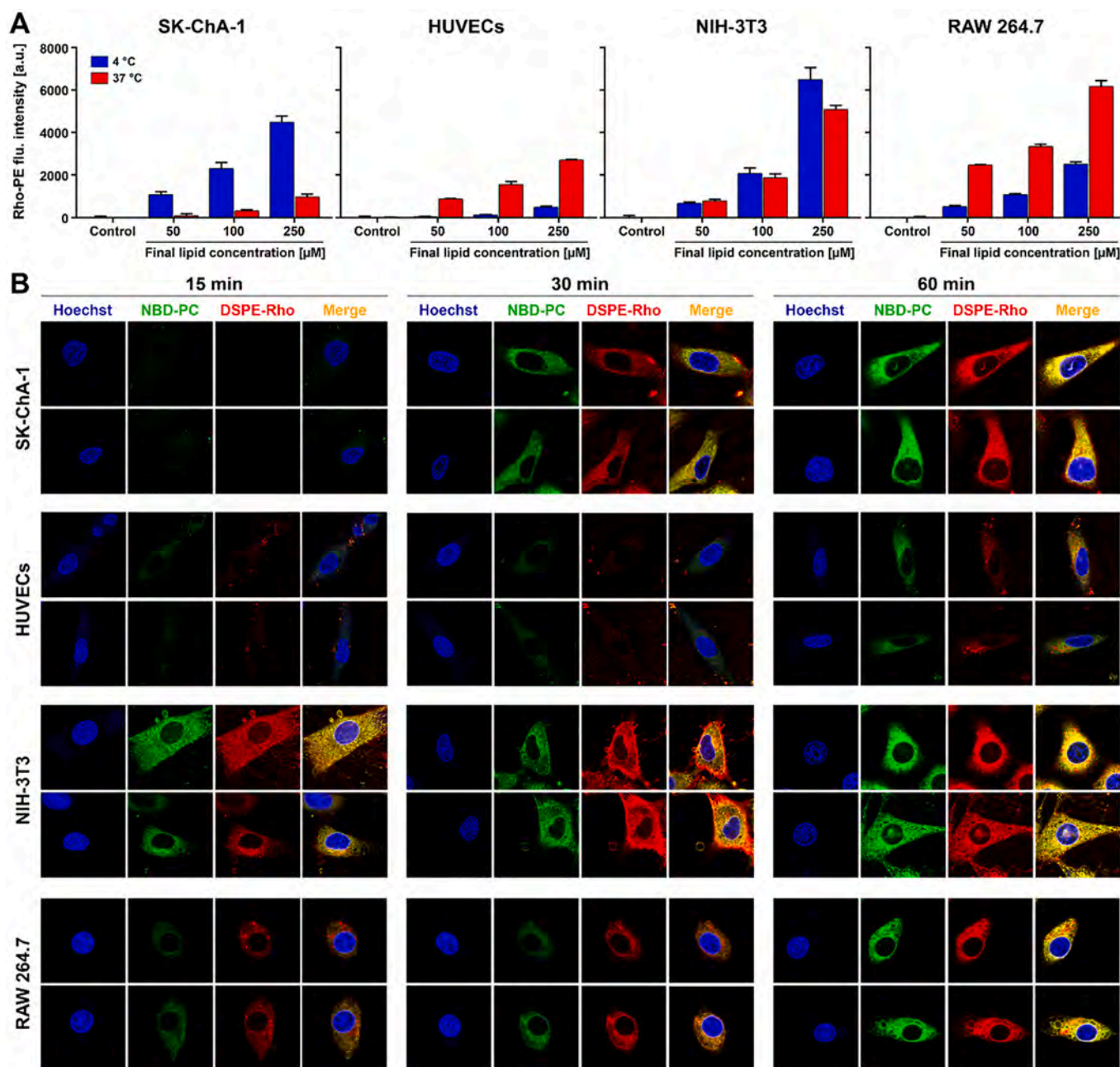


Fig. 2. Uptake and intracellular distribution of fluorescently labeled ITLs in cultured cells. (A) Cells were incubated with 50, 100, and 250 μM of ITLs (final phospholipid concentration) labeled with 1 mol% rhodamine-PE for 2 h at 4 °C and 37 °C. ITL association with cells was analyzed by flow cytometry based on rhodamine-PE fluorescence. Data are presented as mean \pm SD of $N = 3$ experimental replicates per group. (B) Cells were incubated with 250 μM of ITLs (final phospholipid concentration) containing 5 mol% of NBD-PC (green) and 1 mol% of rhodamine-PE (red) for 15, 30, and 60 min, fixed, and imaged by confocal microscopy. Hoechst 33342 was used to stain the cell nucleus (blue) post-fixation. Experimental details are provided in Section 2.5 and S2.5. Images were edited in Adobe Photoshop for hue, lightness, saturation, and contrast in a clustered manner to preserve relative differences in fluorescence intensity. (For interpretation of the references to color in this figure legend, the reader is referred to the web version of this article.)

translocation. Tumors were removed with surgical scissors and tweezers, weighed, and stored at -20°C for future analyses.

2.15. Statistical Analysis

Statistical analysis was performed on Kaplan-Meier data sets in GraphPad Prism. The ZnPC-ITL and AlPC-ITL group was compared to the control group using a log-rank Mantel-Cox test and a Gehan-Breslow-Wilcoxon test. The highest P -value was noted in the results. A P -value of ≤ 0.05 was considered statistically significant.

3. Results and Discussion

In previous work [21] we employed an attritional approach to study the most important aspects of PDT in an *in vitro* setting. The approach was based on association and uptake analyses to determine whether cells were photosensitized, which is essential for a therapeutic effect. When photosensitization was confirmed, the dark toxicity of the PSs was assessed inasmuch as non-illuminated PSs should not be toxic to cells in the absence of light [59] because of non-selective tissue distribution and

uptake [60–62] and hence potential organ damage. When the PSs exerted no dark toxicity, PDT efficacy was confirmed based on cell viability, mode of cell death, and cell cycle arrest assays, i.e., key events in therapeutic tumor killing. A similar approach was applied in the current study and ensued by additional assessment of systemic toxicity and skin phototoxicity *in vivo* to build a preclinical dossier for further translational research prior to clinical trials.

3.1. Tumor-Comprising Cells Take Up ITLs in a Concentration- and Incubation Time-Dependent Manner

Previously it was found that PS-encapsulating ITLs were internalized by cultured biliary cancer (SK-ChA-1) [13,23] and skin cancer (A431) cells [21]. This behavior may not only enable passive targeting of PS to the tumor stroma via the EPR effect [63], but also facilitate subsequent tumor cell photosensitization, which is advantageous in terms of a therapeutic net effect. In the current study, flow cytometry and confocal microscopy imaging were used to verify the uptake of fluorescently labeled ITLs in SK-ChA-1 cells as well as in tumor stromal cells; i.e., fibroblasts (NIH-3T3), endothelial cells (HUVECs), and monocyte/

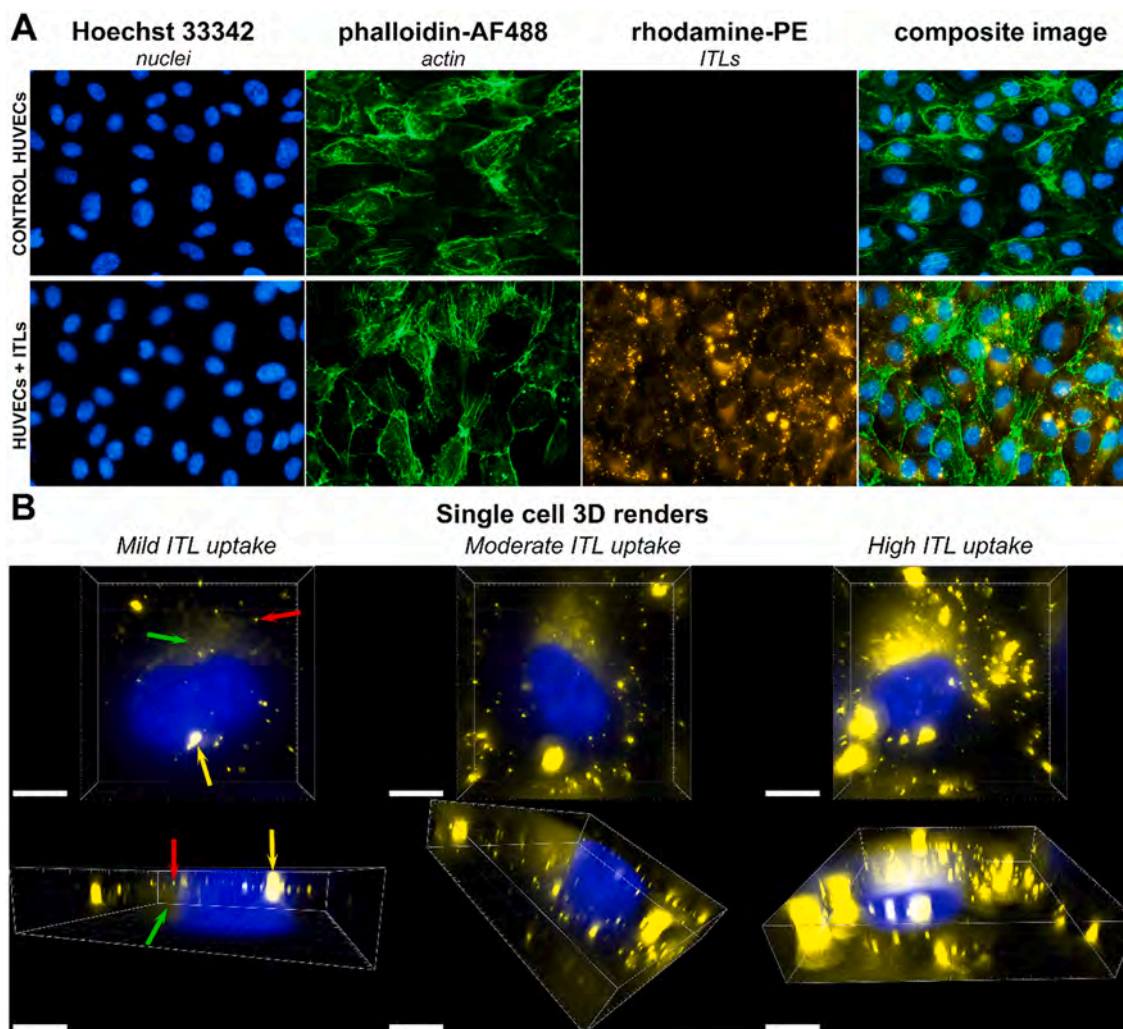


Fig. 3. ITL uptake by endothelial cells under flow conditions. HUVECs were cultured in Ibidi flow chambers under continuous flow conditions for 3 d and subsequently exposed to $150\ \mu\text{M}$ of rhodamine-PE-labeled ITLs (yellow) in EBM-2 medium without growth factors, antibiotics, and serum for 30 min during unidirectional flow (shear rate $300\ \text{s}^{-1}$, shear stress $0.3\ \text{N/m}^2$ ($3.0\ \text{dyn/cm}^2$), viscosity $1\ \text{mPa}\cdot\text{s}$ ($0.01\ \text{dyn}\cdot\text{s/cm}^2$), and a pressure of 9.3 mbar). Cells were fixed and counterstained with phalloidin-AF488 (actin cytoskeleton, green) and Hoechst 33342 (nuclei, blue) and imaged by fluorescence microscopy (A). Control HUVECs were not exposed to ITLs. (B) 3D renders of single cells to demonstrate spatial distribution of rhodamine-PE fluorescence in cells with mild, moderate, and high ITL uptake. Green arrows point to dispersed rhodamine-PE, red arrows indicate small clusters of rhodamine-PE fluorescence, whereas yellow arrows designate large conglomerates of fluorescence. Scale bar = $3\ \mu\text{m}$. (For interpretation of the references to color in this figure legend, the reader is referred to the web version of this article.)

macrophage-like cells (RAW 264.7).

As shown in Fig. 2A, both tumor and non-tumor stromal cells were fluorescently labeled by ITLs after 2-h incubation at 37 °C in a phospholipid concentration-dependent manner. Incubation at 4 °C, at which endocytosis and intracellular transport processes are halted [64,65], augmented the fluorescence staining intensity of SK-ChA-1 cells, had no notable effect in NIH-3T3 cells, and reduced it in HUVECs and RAW 264.7 cells compared to the data at body temperature (Fig. 2A). These findings not only suggest uptake of the ITLs (instead of merely adhesion)

but also indicate that uptake is receptor-mediated in endothelial cells and macrophages but not in cancer cells and fibroblasts. Of note, membrane-membrane contact and subsequent fusion [66] are deterred by the PEG chains, making coalescence of phospholipid bilayers unlikely at 4 °C. Confocal microscopy (Fig. 2B) confirmed that the association observed by flow cytometry was caused by the uptake of the PEGylated liposomes and not merely adhesion to the cells' membrane surface. The uptake mechanism was not further studied at this stage because the in vitro uptake dynamics may misrepresent the more relevant in vivo

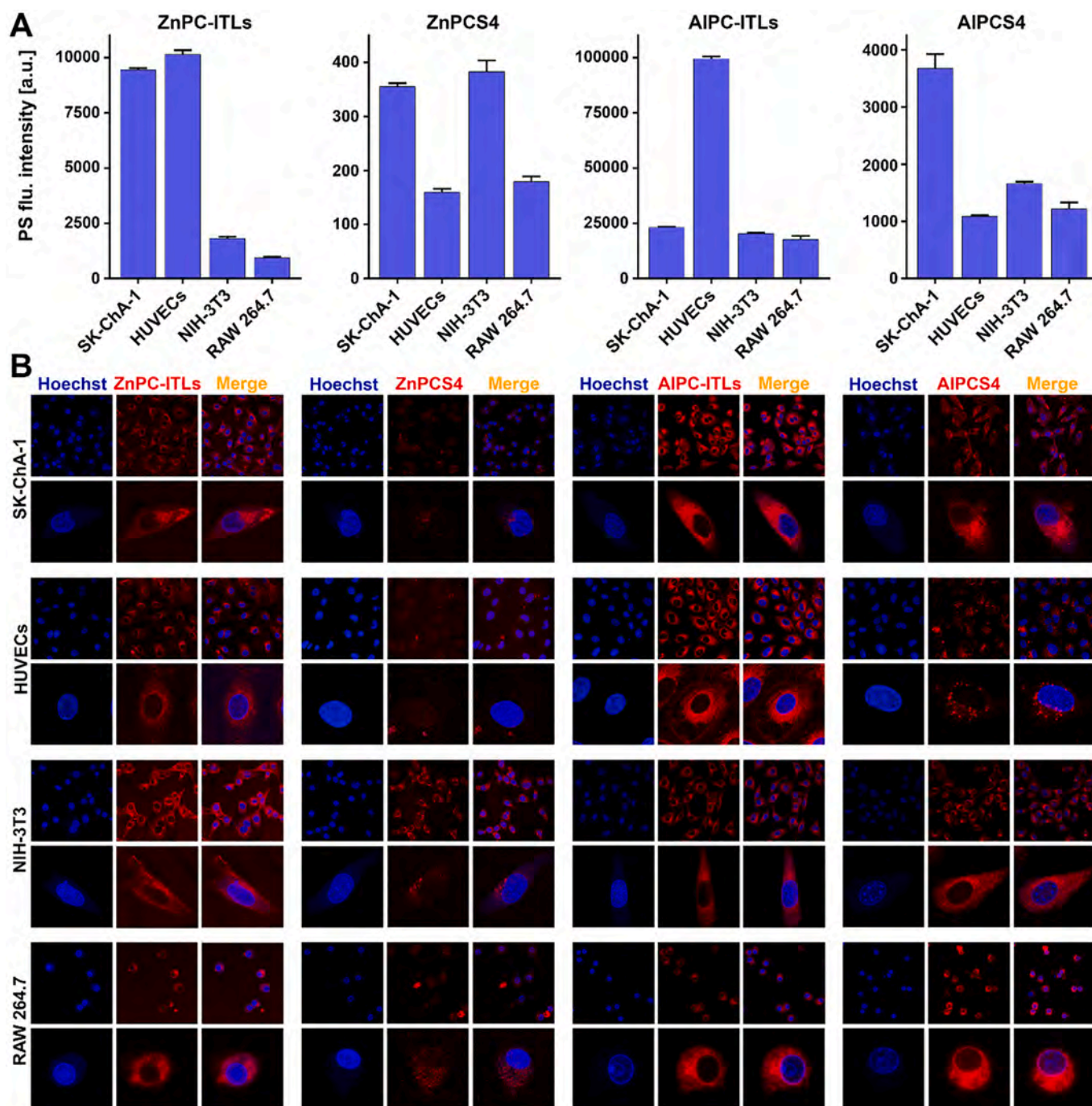


Fig. 4. Photosensitization of cultured cancer cells. (A) Cells were incubated with ZnPC-ITLs or AIPC-ITLs (125- μ M final phospholipid concentration, equating to 0.375- μ M PS concentration) or with 0.375 μ M of ZnPCS4 or AIPCS4 for 60 min under standard culture conditions ($N = 3$ per group) and analyzed by flow cytometry. The fluorescence intensity was background-corrected for cell autofluorescence. (B) Cells were incubated with ITL-delivered ZnPC or AIPC (1000 μ M final phospholipid concentration, equivalent to 3 μ M PS concentration) or with 10 μ M of ZnPCS4 or AIPCS4 for 60 min under standard culture conditions. Following fixation, cells were imaged with confocal microscopy using PS autofluorescence (red). Hoechst 33342 was used to stain nuclei (blue). (For interpretation of the references to color in this figure legend, the reader is referred to the web version of this article.)

cellular internalization processes, which are dominated by the presence and composition of the plasma protein-replete corona covering the PEGylated liposome surface [67]. The unhindered uptake of PEGylated liposomes by cells is in lockstep with other studies [68], and some have even reported increased uptake of nanoparticles as a result of PEGylation [69]. The current findings indicate that cell type is a determinant factor in ITL uptake rate. Fibroblasts had reached a near-saturated state after 15-min incubation while the other cell types exhibited a gradual increase in staining intensity over the course of 60 min. The staining pattern was generally homogeneous across the intracellular space for both fluorescently labeled phospholipids but also revealed localized focal and granular rhodamine-PE concentration. The deviation from the NBD-PC distribution profile indicates differential distribution kinetics of the phospholipids following internalization, which was characteristic for all cell types but was most clearly visible in HUVECs following 60-min incubation (Fig. 2B). In any case, the ITLs were not retained in endosomes as intact particles - a common fate of PEGylated nanocarriers upon endocytosis [70]. A widespread dispersion throughout the cell is potentially beneficial for PDT efficacy with lipophilic PSs as it is expected that multiple cellular structures will be photosensitized. Indeed, multi-site photosensitization leads to the induction of more profound cell death compared to single site photosensitization [20,21].

In contrast to tumor cells, tumor-resident macrophages, and fibroblasts, ITLs interact with endothelial cells under hemodynamic conditions. Accordingly, ITL uptake by cultured HUVECs was assayed in Ibidi flow chambers [36] using parameters that mimic the lower bound flow rates in microvasculature [71] in the absence of plasma proteins and FBS. ITLs were taken up by HUVECs (Fig. 3A) to different degrees (Fig. 3B). The distribution of intracellular fluorescence was comparable to what was observed under static incubation conditions (Fig. 2B), namely patches of homogeneously dispersed rhodamine-PE (Fig. 3B, green arrows) and fluorescence-dense clusters that likely comprise various organelles (Fig. 3B, red and yellow arrows). Photochemical damage to the cell and organelle membranes is expectedly beneficial to indirect tumor killing effects via vascular occlusion, which has been observed following PDT of human tumor xenografts [72] and chicken chorioallantoic membrane vasculature [73]. Photochemical disruption of cell integrity, endothelial cell activation, and exposure of the basement membrane are vaso-occlusive events in that these trigger coagulation and thrombosis [73,74]. The corollary hemostasis then leads to anoxia, metabolic catastrophe [2], and cell death. It remains to be seen what the effect of plasma proteins will be on ITL uptake by HUVECs under flow and hence on photosensitization of tumor endothelium in a normophysiological setting.

3.2. Tumor-Comprising Cells are Ubiquitously Photosensitized by Liposomal and Tetrasulfonated Metallated Phthalocyanines

After confirming the uptake of the liposomal constituents of ITLs by target cells, we investigated whether and to what extent liposomal PS delivery occurred and how the PS molecules were distributed intracellularly. Photosensitization by water-soluble ZnPC and ALPC derivatives was also determined. Photosensitization was screened using PS autofluorescence [21]. It should be noted that, since the photophysical and photochemical properties differ among the PSs, only intragroup comparisons can be made [20,21].

All cell types had internalized PS molecules during 60-min incubation but the level of photosensitization was PS- and cell type-dependent (Fig. 4A). No plateau in intracellular PS concentration was reached during 60-min incubation in any of the cell types (Fig. S6). For the ITLs it was hypothesized that the degree of photosensitization would be proportional to the intensity of phospholipid fluorescence. However, this hypothesis was nullified, as for example RAW 264.7 macrophages exhibited the most intense rhodamine-PE fluorescence (indicating greatest ITL internalization; Fig. 2A) but the lowest ZnPC and ALPC fluorescence (indicating lowest photosensitization). The disconnect

could not be explained by technical reasons given that the uptake experiments had been performed under the same conditions. Moreover, it is unclear why a change in the central core elements of the PSs (chloro (29H,31H-phthalocyaninato)aluminum vs. zinc phthalocyanine), which is located in the most lipophilic region of the lipid bilayer with no direct impact on membrane-membrane interactions, would have a profound effect on cell uptake (see uptake of ZnPC-ITLs in SK-ChA-1 cells vs. HUVECs compared to the uptake of ALPC-ITLs in those cells; Fig. 4A). Stark differences also manifested at the level of intracellular distribution kinetics. ITL-delivered ZnPC accumulated in the cell membrane during the first 30 min of incubation and gradually scattered across the rest of the cellular milieu in the subsequent 15 min (Figs. S7–9). Contrastingly, ITL-delivered ALPC had already homogeneously diffused throughout the cell at the 15 min assessment point (Figs. S7–9). The implications of these observations should be considered when designing *in vitro* experiments since intracellular PS localization and mode of cell death are interrelated [20]. Some PSs require >60 min to reach uniform distribution in cells.

Nevertheless, the intracellular PS distribution patterns after 60 min of ITL exposure (Fig. 4B) were comparable to the labeled phospholipid distribution patterns (Fig. 2B). In fact, both types of PSs were replete throughout the cell with a few notable exceptions addressed below, whereby ZnPC and ALPC occupied lipophilic domains and ZnPCS4 and ALPCS4 were enriched in the hydrophilic regions of the cell based on their chemical properties [20]. ZnPCS4 has a low fluorescence quantum yield and was therefore difficult to image. ZnPC distribution appeared more granular than ALPC distribution in SK-ChA-1 cells, implying that ZnPC may be enriched in organelles relative to other structures in cancer cells. Almost exclusive endovesicularization was noted for ALPCS4 in HUVECs, suggesting pinocytotic uptake and endosomal confinement of the PS. In contrast, the other cell types exhibited pleiotropic distribution of ALPCS4. Homogeneous distribution patterns were also observed in SK-ChA-1 cells [23] and human epidermoid carcinoma (A431) cells [21] and therefore appear to be the main dispersion mode. As alluded to previously, multitargeted cytosolic photosensitization is desirable for optimal PDT efficacy.

3.3. Lipophilic and Hydrophilic Metallated Phthalocyanines Exhibit No-to-Moderate Dark Toxicity

The toxicity of PSs in the absence of light was determined using the WST-1 assay, reflecting the mitochondrial redox potential, and the SRB assay, which is a measure of the total protein content. In principle, afflicted cells undergo mitochondrial perturbation and uncoupling of the electron transport chain before detaching from the well surface, so the assays reflect early and late events in the death cascade.

At the longest incubation time (3 d) and highest concentration (Fig. 5), none of the PSs exerted toxicity in cancer cells, which is consistent with earlier reports on SK-ChA-1 cells [13,23] and A431 cells [21]. The non-cancerous cells were more susceptible to the PSs. ZnPCS4 showed the highest toxicity (SRB assay) in endothelial cells, fibroblasts, and macrophages. Toxicity generally set in or was exacerbated after longer incubation times and higher PS concentrations (Figs. S10 and S11). The degree of toxicity was mild-to-moderate in the non-cancerous cells. It should be noted that the experiments were performed in medium^{-/-} that lacked FBS. Although this did not affect cancer cells, the absence of FBS may have rendered the non-cancerous cells more vulnerable to stress - in this case from potentially toxic compounds - and may hence be an overestimation of toxicity before illumination. Naturally, after PDT the liposomal constituents and PSs will remain in the non-cancerous cells and could, based on the data in Fig. 5, confer an additional boost in toxicity in photochemically damaged cells suffering from hyponutrition and metabolic crisis.

It is questionable whether the tumor-comprising cells will reach the ITL exposure levels *in vivo* as applied in the *in vitro* assays. As summarized in [49], liposomal formulations are injected into animals at a

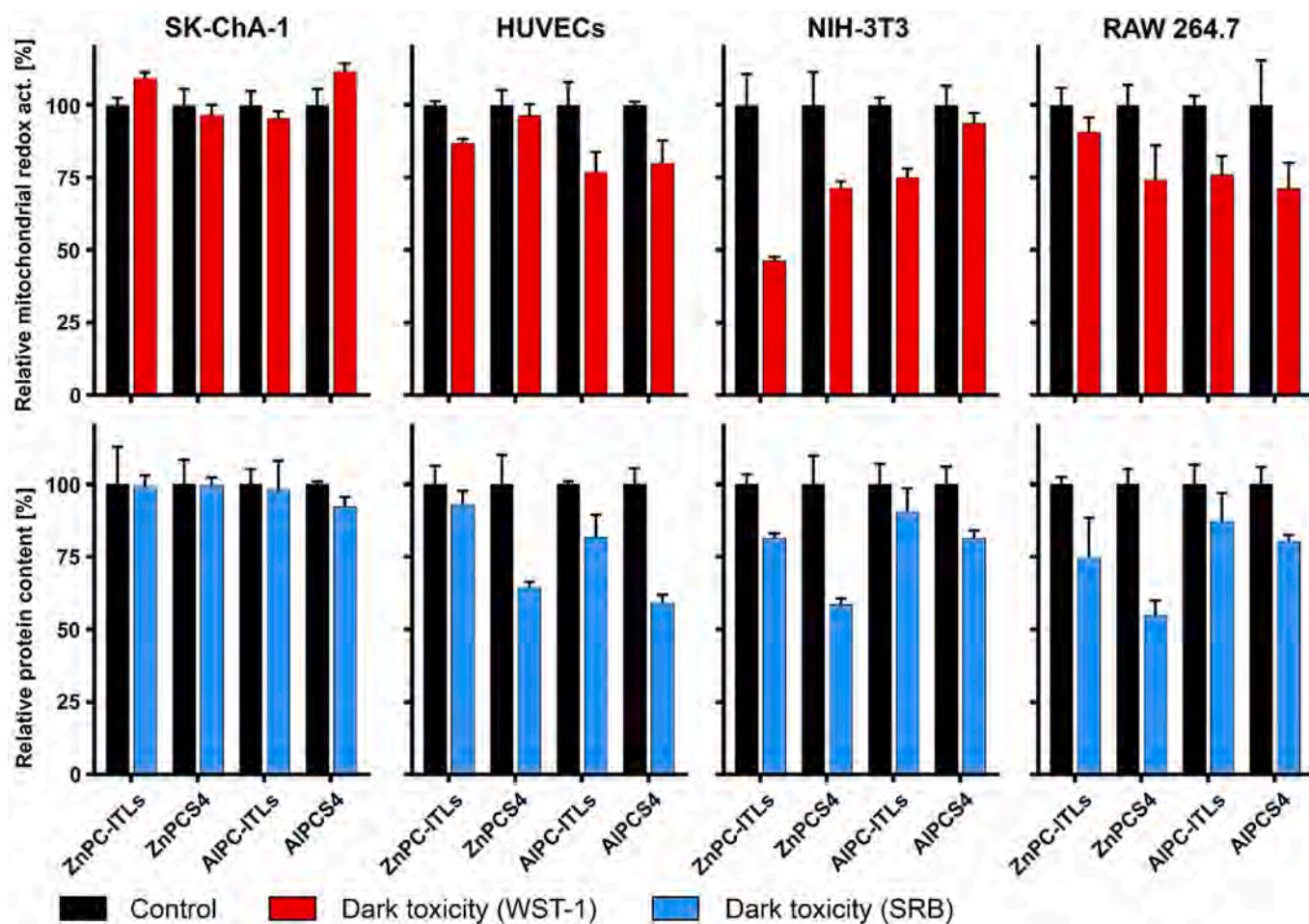


Fig. 5. Dark toxicity in cultured tumor-comprising cells. SK-ChA-1, HUVECs, NIH-3T3, and RAW 264.7 cells were incubated with 500 μM of ZnPC-ITLs and AIPC-ITLs (equivalent to 1.5- μM PS concentration) or 10 μM of ZnPCS4 and AIPCS4 for 72 h in the dark under standard culture conditions. Toxicity was analyzed using a WST-1 assay (mitochondrial activity; red bars) followed by the SRB assay (total protein content; blue bars). Cells in the control group were not exposed to PSs. Individual results were normalized to the mean of the control group. Data are reported as mean \pm SD for $N = 3$ independent experiments per group. Readers are referred to Figs. S10 and S11 for dark toxicity at earlier time points and lower PS concentrations. (For interpretation of the references to color in this figure legend, the reader is referred to the web version of this article.)

Table 1

PDT-mediated half maximum lethal concentration (LC_{50}) of lipophilic and hydrophilic metalated phthalocyanines.

PS	Cell type	WST-1		SRB	
		Incubation time [h]		Incubation time [h]	
		4 h	24 h	4 h	24 h
ZnPC (ITLs)	SK-ChA-1	0.22 \pm 0.01	0.25 \pm 0.01	1.14 \pm 0.15	0.16 \pm 0.02
	HUVECs	3.93 \pm 0.93	4.04 \pm 0.75	2.27 \pm 0.47	1.87 \pm 0.16
	NIH-3T3	5.72 \pm 1.38	0.60 \pm 0.04	3.17 \pm 0.52	2.03 \pm 0.42
	RAW 264.7	0.62 \pm 0.03	0.48 \pm 0.01	1.12 \pm 0.03	0.91 \pm 0.07
ZnPCS4	SK-ChA-1	26.0 \pm 0.60	N.D.	18.1 \pm 1.30	N.D.
	HUVECs	N.D.	N.D.	N.D.	25.7 \pm 0.80
	NIH-3T3	N.D.	N.D.	N.D.	N.D.
	RAW 264.7	N.D.	N.D.	N.D.	N.D.
AIPC (ITLs)	SK-ChA-1	0.35 \pm 0.20	0.05 \pm 0.01	0.97 \pm 0.18	0.01 \pm 0.00
	HUVECs	0.21 \pm 0.01	0.19 \pm 0.01	0.68 \pm 0.17	0.41 \pm 0.08
	NIH-3T3	0.52 \pm 0.02	1.53 \pm 0.05	1.59 \pm 0.11	1.73 \pm 0.20
	RAW 264.7	1.66 \pm 0.09	0.98 \pm 0.04	1.66 \pm 0.08	1.34 \pm 0.03
AIPCS4	SK-ChA-1	0.29 \pm 0.01	0.16 \pm 0.01	0.50 \pm 0.05	0.16 \pm 0.04
	HUVECs	0.20 \pm 0.01	0.16 \pm 0.01	9.80 \pm 0.70	0.05 \pm 0.03
	NIH-3T3	0.11 \pm 0.02	0.13 \pm 0.02	N.D.	N.D.
	RAW 264.7	0.15 \pm 0.01	0.36 \pm 0.02	0.33 \pm 0.04	4.80 \pm 0.20

The LC_{50} values (in μM) were calculated from the non-linear fit function (Figs. S12 and S13) and are given as mean \pm SD of $N = 3$ independent experiments per group.

plasma concentration of maximally 3 mM phospholipids. It is therefore improbable (and unfortunate) that passively targeted ITLs will attain an intratumoral concentration of 0.5 mM (i.e., ~15% of total injected dose), especially since comparable formulations of doxorubicin (Caelyx) accumulate in the tumor at a ~4% fraction of the injected dose after 24-h and 48-h circulation [75]. The highest evaluated phospholipid concentration is even more unlikely to be achieved in the plasma of human patients because that would require the administration of a large volume of a highly concentrated liposomal suspension. Consequences for non-malignant endothelial cells, fibroblasts, and macrophages that the injected liposomes come in contact with are therefore unwarranted. Accordingly, the *in vitro* toxicity results pose no practical concern at this stage with respect to the ITL formulations.

For the water-soluble AlPCS4 the systemic concentration can be easily increased compared to what was used in the *in vitro* dark toxicity studies, although toxicity to non-cancerous cells should be taken into account. In unpublished pilot experiments we injected 2 $\mu\text{mol}/\text{mouse}$ and 1 $\mu\text{mol}/\text{mouse}$ of AlPCS4, which translates to a systemic concentration of 1.2 mM and 0.6 mM at a blood volume of 80 $\mu\text{L}/\text{g}$ body weight. These high concentrations resulted in 100% (3/3) and 67% (2/3) mortality 24 h after intravenous administration. Consequently, *in vivo* toxicological testing was performed in two animal models below to curtail any detrimental systemic effects of the PS before PDT *in vivo*.

3.4. All PSs except ZnPCS4 Exhibit Strong-to-Potent Toxicity in Illuminated Tumor-Comprising Cells

PDT was performed at the same settings as in the previous study with A431 cells [21] to make comparative analysis possible. In A431 cells and the cell lines investigated in the present experiments, PDT with ZnPCS4 conferred no notable light-mediated toxicity (Table 1) [21], which is in agreement with the inability of ZnPCS4 to generate ROS upon illumination [20] and the absence of protein oxidation (Fig. S14). ZnPCS4 was therefore deemed ill-suited for further development of the PDT platform [21], corroborated here. When grouped, the remaining PSs were associated with the following mean \pm SD LC_{50} values: 1.17 \pm 1.80 μM (range 0.11–5.72 μM), WST-1 at 4 h; 2.11 \pm 2.68 μM (range 0.50–9.80 μM), SRB at 4 h; 0.74 \pm 1.12 μM (range 0.05–4.04 μM), WST-1 at 24 h; and 1.22 \pm 1.41 μM (range 0.01–4.80 μM), SRB at 24 h. Compounds with an LC_{50} value of <1 μM were classified as potent, whereas compounds with an LC_{50} in the range of 1–20 μM were classified as having very strong toxicity [76]. ZnPC-ITLs, AlPC-ITLs, and AlPCS4 gyrated between these classifications depending on the cell line, assay method, and the time interval between treatment and assessment. The PSs can therefore be considered good-to-excellent oncotherapeutics in the framework of our comprehensive PDT platform targeting the most important tumor-comprising cells.

From the dark toxicity (Figs. 5, S10, S11) and LC_{50} values (Table 1), a selectivity index (SI) can be extrapolated. In the context of PDT, the SI can be defined as the ratio of the PS's dark toxicity concentration against its pharmacologically active concentration [77]. The ideal PS should have a relatively high dark toxicity concentration and a very low photoactive concentration [78]. For anti-cancer pharmaceuticals, an SI value of ≥ 10 is deemed worthy of further investigation [79]. To approximate the SI, the most profound dark toxicity was determined per PS in each cell line irrespective of post-PDT incubation time (Figs. S10 and S11) and the corresponding PS concentration was divided by the LC_{50} value at 24 h (Table 1) in an assay-matched manner (i.e., WST-1 dark toxicity versus WST-1 LC_{50}). The dark toxicity LC_{50} values were calculated where necessary, assuming a linear concentration-toxicity relationship. For ZnPC-ITLs, the mean \pm SD [range; percentage of data points with SI ≥ 10] SI was 1.8 \pm 1.8 [0.2–3.1; 0%], indicating that this PS and delivery system combination may be too toxic in the absence of a light stimulus. For AlPC-ITLs the SI values were 11.2 \pm 20.1 [0.2–55.9; 29%], whereas for AlPCS4 the SI values were 72.9 \pm 72.6 [0.2–212.7; 71%], reflecting a higher safety profile compared to the zinc-containing

PC counterpart. Only certain cells were too susceptible to aluminum-containing PCs. AlPC-ITLs and AlPCS4 were least tolerated by macrophages, which may in fact be advantageous for PDT. It is known that tumor-associated macrophages of the M2 phenotype inhibit T cell-mediated anti-tumor immune responses [80] and that the T cell response that is inherent to post-PDT immune signaling is quintessential for tumor clearance and long-term tumor control [4,5,81]. By inflicting toxicity in M2 macrophages via inherent PS dark toxicity the post-PDT immune response may be exacerbated, on top of being triggered by the M2 to M1 phenotype switch by PDT itself [82]. Contrastingly, the M1 phenotype is hostile towards tumor cells [80]. PDT with aluminum-containing PCs may therefore relay a beneficial kill-and-switch effect in tumor-associated macrophages.

Several other conclusions can be derived from the data. Firstly, there was no correlation between the extent of photosensitization (based on PS fluorescence intensity measured by flow cytometry) and 24-h LC_{50} values when the data were ranked per individual PS for the 4 cell lines. For example, HUVECs had top rank in terms of ZnPC-ITL uptake (Fig. 4A) but bottom rank with respect to LC_{50} (WST-1; Table 1). In fact, only 2 of the 24 matrix entries had equal rank (ZnPC-ITLs, uptake versus WST-1 LC_{50} in NIH-3T3 cells; AlPCS4, uptake versus SRB LC_{50} in RAW 264.7 cells). Accordingly, PS uptake has no prognostic value for PDT efficacy. Secondly, cancer cells tested to date have proven to be highly amenable to PDT with the metallated PSs, with a mean \pm SD LC_{50} value of 0.30 \pm 0.41 when the LC_{50} values for A431 cells [21] and SK-ChA-1 cells (this study) were grouped for the WST-1 and SRB assay performed at 24 h post-PDT. These LC_{50} values belong in the potent anti-cancer agent stratum [76]. Parenchymal cells are the primary targets in the PDT platform, with the other pharmacologically relevant loci acting as 'adjuvant targets' [21]. Finally, AlPCS4 inflicted the most profound damage across the board with very low LC_{50} values based on the WST-1 assay, which relies on mitochondrial redox potential [83]. AlPC-ITLs were slightly more phototoxic to cells than ZnPC-ITLs, although both PS also performed well in terms of cell-killing potency. Hybrid modalities should therefore be considered comprising ITL-delivered lipophilic PS such as AlPC-ITLs to target membrane structures and hydrophilic AlPCS4 to target the aqueous compartments of the cell, with the aim to induce maximal photochemical damage to the widest possible range of biomolecules.

3.5. ITL-Delivered Metallated Phthalocyanines are More Potent Inducers of Cell Cycle Arrest, Apoptosis, and Necrosis

Cell cycle stages and mode of cell death were measured following the protocol used previously for A431 cells [21] as a metric of the PSs' phototoxicity, secondary to the WST-1 and SRB data. Furthermore, the mode of cell death, which is a culminant of cell cycle arrest, is a gauge for a cell's ability to recover and dictates post-PDT immunological clearance. Sublethally afflicted cells can cope with hyperoxidative stress by activating survival pathways [2,13–16] that lead to anastasis (cell survival and recovery through reversal of apoptosis) [84] and other forms of post-traumatic recovery [85–87]. These processes require energy in the form of ATP. Apoptosis, necroptosis, secondary necrosis, and paraptosis are also energy-demanding cell death cascades. Cells undergoing a predominantly apoptotic mode of cell death (AV+/PI-) are therefore fundamentally capable of reverting death signals and recover. Contrastingly, necrosis results from energy depletion and is not compatible with recovery. The mode of cell death in turn shapes the anti-tumor immune response [88], which is required for long-term tumor control [81,89], and abscopal effects [90] that bear clinical relevance in cases of viable tumor residuals post-PDT and (micro)metastases that may have escaped detection by imaging.

PDT generally resulted in an increase in the fraction of cells arrested in the S-phase and G₂/M-phase (Fig. 6). The extent to which S-phase and G₂/M-phase arrest occurred depended on the type of PS, with ITL-delivered lipophilic PSs inducing more profound cell cycle arrest than

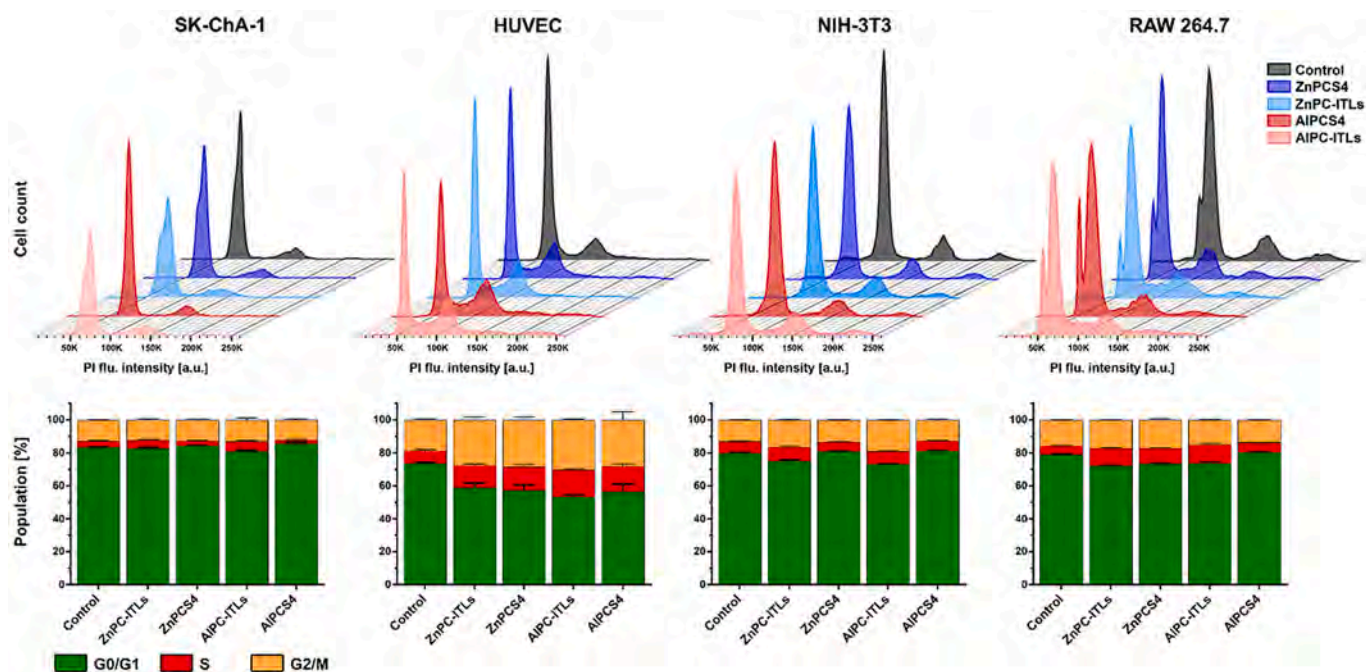


Fig. 6. Cell cycle profile in PDT-treated tumor-comprising cells. Cells were photosensitized with ZnPC-ITLs and AIPC-ITLs (31.25 μM phospholipid concentration, 0.09 μM PS concentration) and ZnPCS4 and AIPCS4 (0.31 μM) during 60-min incubation under standard culture conditions. Cells were illuminated (cumulative radiant exposure of 15 J/cm^2), harvested 24 h after PDT, fixed, and stained with PI before flow cytometry. Data are presented as mean \pm SD for $N = 3$ independent experiments per group.

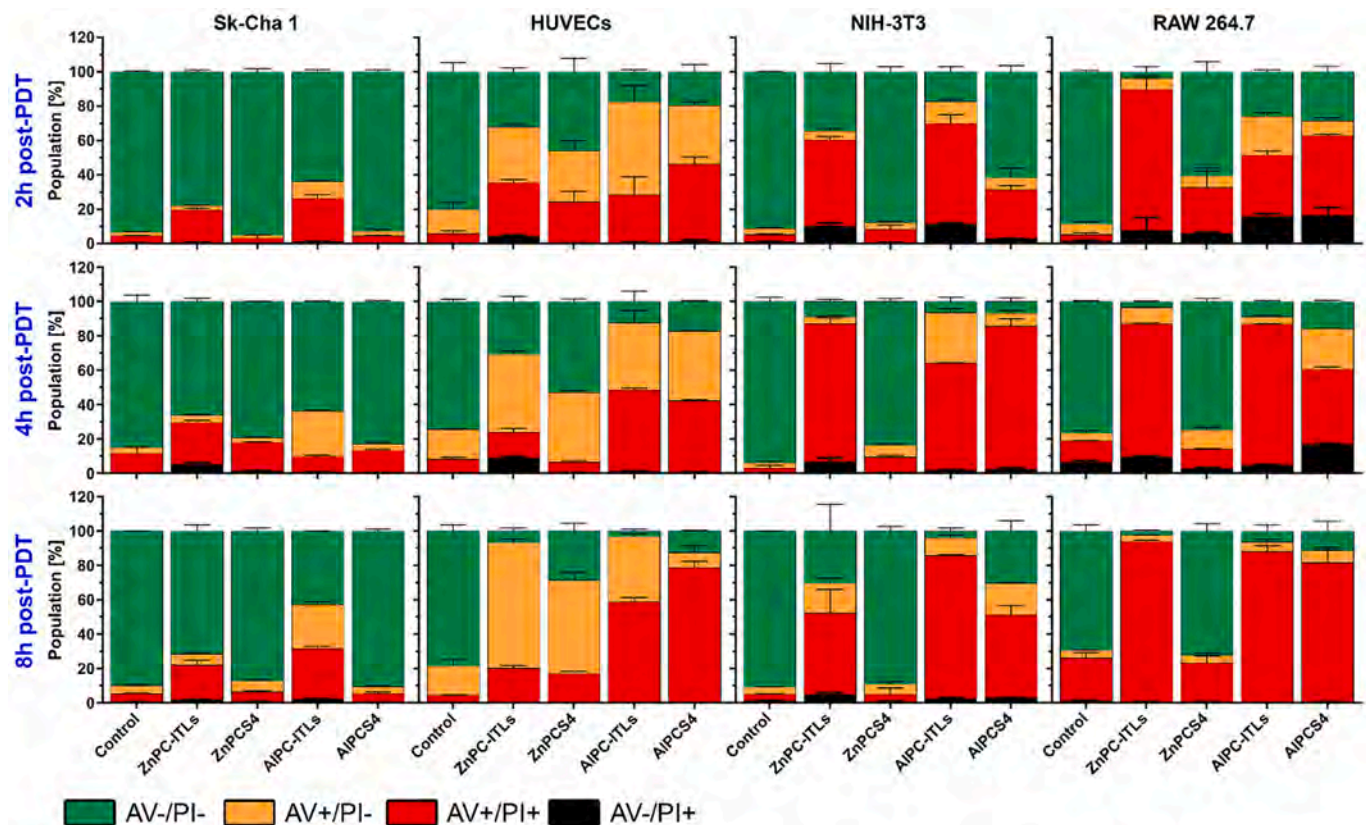


Fig. 7. Mode of cell death in PDT-treated tumor-comprising cells. Cells were photosensitized with ZnPC-ITLs and AIPC-ITLs (250 μM phospholipid concentration, 0.75 μM PS concentration) and ZnPCS4 and AIPCS4 (2.5 μM) during 60-min incubation under standard culture conditions. Cells were stained with PI and Alexa Fluor 488-conjugated annexin V (AV) at 2, 4, and 8 h of post-PDT (cumulative radiant exposure of 15 J/cm^2) and assayed by flow cytometry. Data are presented as mean \pm SD for $N = 3$ independent experiments per group. Corresponding quantitative data are provided in Table S6. Classification: AV-/PI-, viable cells; AV+/PI-, early apoptotic cells; AV+/PI+ and AV-/PI+, cells in late apoptosis or necrosis.

their hydrophilic counterparts at roughly 3-fold lower PS concentration. Moreover, the non-cancerous cells, and HUVECs in particular, displayed greater cell cycle arrest (Fig. 6) than the SK-ChA-1 cells, while the LC_{50} values in the former cells were typically higher than in SK-ChA-1 cells (Table 1) as well as A431 cells [21]. Similar trends in LC_{50} values were found for apoptosis/necrosis (Fig. 7). These data represent another example of the disconnect between inter-assay results. Plausible explanations are that post-PDT recovery processes in the non-cancerous cells are more resolute than in the cancer cells, that cancer cells become more frail than non-cancerous cells when serum-deprived, and/or that paracrine death signaling loops are more detrimental in cancer cells (e.g., through PDT-induced tumor necrosis factor (TNF) release and locoregional signal transduction [24,91]). It is known that serum deprivation, as implemented here and in our previous studies [14,15,21], arrests certain cells in the G_0/G_1 -phase, including fibroblasts [92,93] and cancer cells [94,95]. A double-digit percentual increase in G_0/G_1 -phase arrest following 24-h serum starvation has been reported in cancer cells [95], leading some to propose this form of metabolic deprivation as a potential therapeutic avenue [96]. This avenue is particularly pertinent

to PDT when the treatment leads to vascular shutdown, as multiple metabolic hubs in cancer cells become congested in consequence to the direct photodynamic effects on cells [2] and hence could account for synergism in treatment efficacy. The serum deprivation-enhanced sensitivity of G_0/G_1 -phase-arrested cancer cells was reported to emanate from signaling by TNF-related apoptosis-inducing ligand (TRAIL) [96], a protein that binds to the death receptors (DR)4 and DR5 and induces apoptosis. Moreover, PDT can invoke susceptibility of TRAIL-resistant cancer cells to TRAIL [97] while at the same time increasing TRAIL release by PDT-treated cells [98], creating another paracrine death signaling loop. It should be noted, though, that HUVECs and RAW 264.7 cells were not considerably affected by serum deprivation and G_0/G_1 -phase arrest per se inasmuch as such an arrest would preclude the cells from being arrested in the S-phase (both HUVECs and RAW 264.7 cells) and the G_2/M -phase (mainly HUVECs) after PDT (Fig. 6).

The cell cycle arrest patterns (Fig. 6) were broadly reflected in the cell death patterns in isolated cell lines (Fig. 7). Most notably, the non-cancerous cells exhibited more apoptosis and necrosis after PDT than

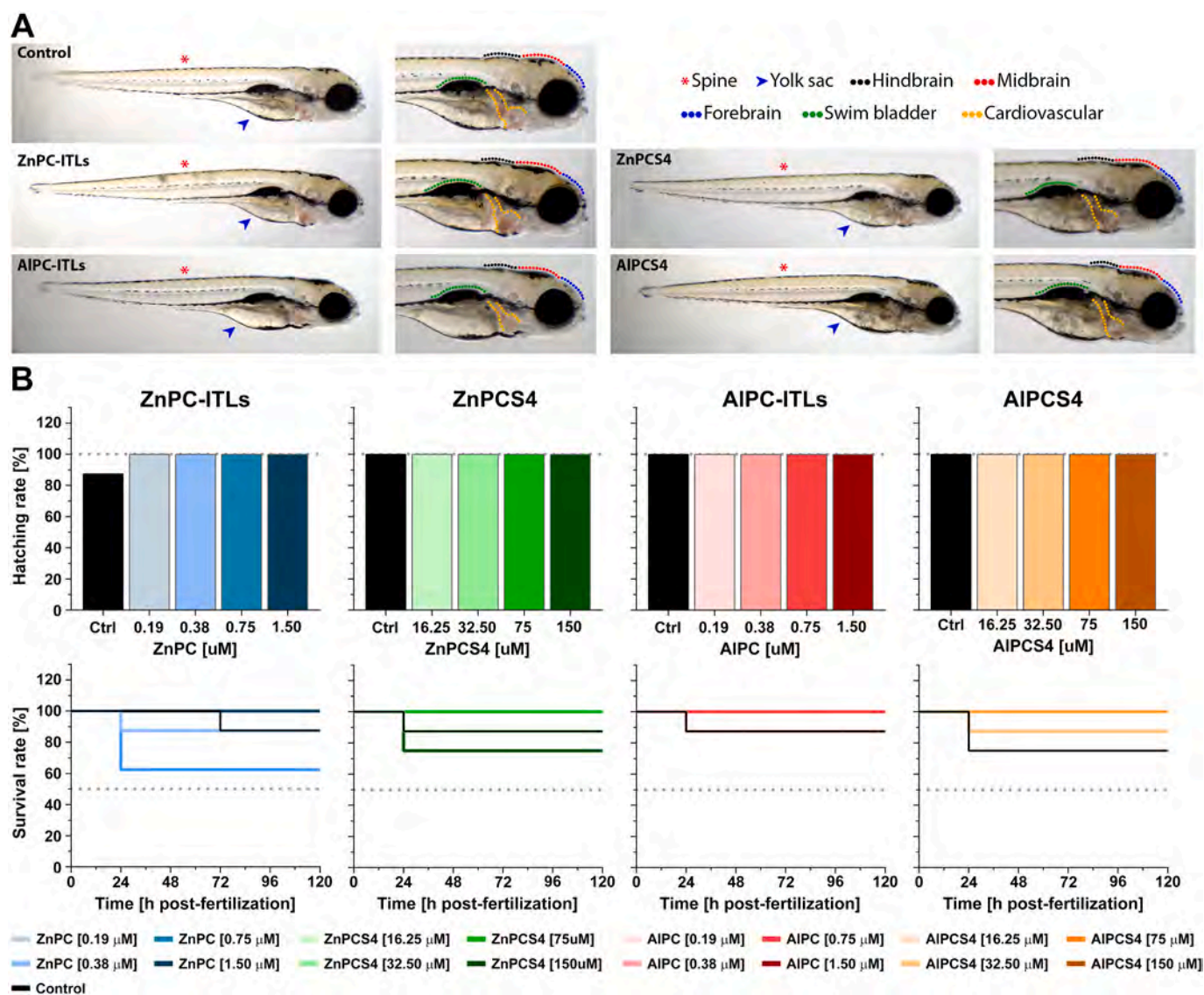


Fig. 8. Systemic toxicity in zebrafish. (A) Representative whole-body images and magnified snapshots of hatched zebrafish indicate no anatomical anomalies at key locations where drug toxicity is expected to manifest (legend top right). Images were taken at 120 h post-fertilization after embryos had been exposed to 1.5 μ M ZnPC and AIPC or 150 μ M ZnPCS4 and AIPCS4. (B) Hatching rate (top panel) as a function of PS concentration ($N = 8$ per concentration) and survival rate (bottom panel) plotted as a function of time ($N = 8$) for the highest PS concentration measured in each group.

SK-ChA-1 cells. The fraction of cells undergoing any mode of cell death increased with time after PDT. The ITL-delivered PSs were more phototoxic than their hydrophilic counterparts, with ALPC being a more potent inducer of cell death than ZnPC except in RAW 264.7 macrophages, echoing previous results in A431 cells [21]. ZnPCS4 imparted no cytotoxicity in cells except in HUVECs, where cell death was disproportionately sizeable and dominated by apoptosis. Previous studies in cancer cells such as A431 cells [99,100] have demonstrated phototoxic responses to ZnPCS4, which were ascribed to possibly the formation of oxygen-free radicals [101], but which could not be reproduced in our previous work at the level of radical production [20] and cellular phototoxicity [21]. Although it is peculiar why oxygen-free radicals would be toxic to select cells (radicals react with electron acceptor sites on any biomolecule), the cytotoxicity of ZnPCS4 in HUVECs was significant enough to warrant *in vivo* investigation as a selective tumor endothelium PS. Necrotic cell death constituted the main mode of cell death in all cell types but HUVECs, the only primary cells in this study. At the earlier time points (2 h and 4 h post-PDT) a remarkable fraction of cells was AV-/PI+, suggesting that PDT induced temporary membrane permeability allowing PI to enter the cell and stain DNA. The membrane permeability abated in time (8 h post-PDT). The early-onset permeability of the outer membrane, albeit transient, may have contributed to cell death - predominantly necrosis - as a result of perturbation of cellular homeostasis [102]. These phenomena are reminiscent of ferroptosis, characterized by the accumulation of oxidized polyunsaturated fatty acids and inherently linked to PDT [103].

In the attritional study conducted in A431 cells [21] it was determined that ALPC-ITLs comprised the most suitable PS delivery system for PDT, with ALPCS4 as a possible co-PS for the pleiotropic photosensitization of the intracellular environment. Given the dark toxicity data, intracellular PS distribution pattern, and photo-induced toxicity it can be surmised that the previous conclusion was reassessed in this study, noting that ZnPC-ITLs were not considerably inferior to ALPC-ITLs.

3.6. Liposomal Photosensitizers and ALPCS4 Exhibit Minimal Dark Toxicity in Zebrafish and Chicken Embryos

To get more insight into the *in vivo* application of the PSs, dark toxicity was measured in zebrafish and chicken embryos. Zebrafish share many toxicological pathways with mammals and therefore constitute a reliable means to assess the hazards that a drug could pose to humans [104]. Chicken embryos are equally suitable test systems [105], especially because they are more sensitive indicators of drug toxicity owing to low-threshold lethality.

Zebrafish embryos were exposed to up to 1.5 μM of liposomal ZnPC and ALPC and up to 150 μM ZnPCS4 and ALPCS4. No morphological or

teratogenic abnormalities were observed in any of the fish (Fig. 8A and S3), and no aberrant zebrafish hatching (determined 72 h post-hatching) or lethality were observed between day 1 and day 5 regardless of PS concentration (Fig. 8B). Lethality was mainly noted in the first 24 h, which was equally divided over all groups, with the sole exception of the 0.75 μM ZnPC group, and was not dose-dependent (Fig. 8B).

Chicken embryos received a single bolus of PS in iso-osmolar buffer solution via the chorioallantoic membrane vasculature on EDD10 to actualize systemic exposure to 0.8 μM ZnPC and ALPC (injected dose of 1.2 nmol) and 85 μM ZnPC and ALPC (injected dose of 128 nmol). The embryos were screened for viability on a daily basis up to EDD18. As presented in Fig. 9, the only PS that induced notable toxicity was ZnPCS4, while the other PSs were more or less comparable to the respective control groups.

The toxicity determined in both animal models was less grave than initially reflected by the dark toxicity results in cultured non-cancerous cells (Fig. 5). Non-cancerous cells were exposed to an equimolar concentration of liposomal ZnPC and ALPC (in zebrafish) and a 15-fold and 8.5-fold lower tetrasulfonated PS derivative concentration (in zebrafish and chickens, respectively). Each PS exhibited some level of toxicity with up to ~50% cell death (NIH-3T3, ZnPC-ITLs, WST-1 assay); a degree that was not observed in animals. The data suggest that dark toxicity assessment in cultured cell monolayers may lead to an overestimation of toxicity, and that therefore *in vitro* toxicological studies constitute a more sensitive gauge. On the other hand, transcriptomics analyses in SK-ChA-1 cells revealed no dysregulation of any of the microarrayed genes by ZnPC-ITLs in the absence of light [13], albeit the exposure time was significantly shorter (2 h) than used here (72 h). Nevertheless, transcriptomic processes are typically very sensitive to external stimuli with detectable early-onset modulation, as was evident from the vast array of changes induced by sublethal PDT at the 90 min post-PDT mark [13] and with cationic liposomes in the absence of light (manuscript in preparation). Furthermore, chicken embryos could withstand all ZnPC-ITL concentrations, although these were three-fold lower than what had been previously tested (up to 0.7 mM systemic lipid concentration, 2.1 μM ZnPC concentration) [13]. In mice, a single intravenous bolus of ZnPC-ITLs (2.5-mM final lipid concentration and 7.5- μM ZnPC concentration in blood) resulted in no body weight alterations during the 4-wk monitoring period, no deleterious changes in clinical biochemistry and hematological parameters, and no histological anomalies at animal sacrifice (4 wk after intravenous administration). Accordingly, the photosensitization protocol to be used for *in vivo* PDT efficacy studies is not expected to produce a level of systemic toxicity in mouse models that would constitute a stop signal for further investigations.

3.7. *In Vivo* Skin Phototoxicity Manifested in Nude Mice Exposed to ZnPC and ZnPCS4 but Not ALPC and ALPCS4

In addition to systemic toxicity, skin phototoxicity is a potentially serious side-effect of clinical PDT that is experienced by some patients even long after PS administration (Fig. 10). In fact, based on the cases presented in Fig. 10, the short median survival time of hilar cholangiocarcinoma patients, and the recommended post-PDT dark periods for clinical PSs, the gastroenterologist decided to discontinue PDT for said patients at our institute [20]. Preventing ambient/sun light-induced burns and photo-allergic reactions should therefore be routinely investigated in preclinical research to minimize sequelae in subsequent clinical trials and ultimately increase adoption of the modality by physicians, especially since PDT can increase median life expectancy of cholangiocarcinoma patients compared to palliative chemotherapy [38,39].

To this end, we have designed a simple yet useful skin phototoxicity setup (Fig. 1) and assessment approach, where we can determine light-induced macroscopic damage in mouse ears and microscopic damage at the histological level in dorsal skin following 24-h exposure to light of a

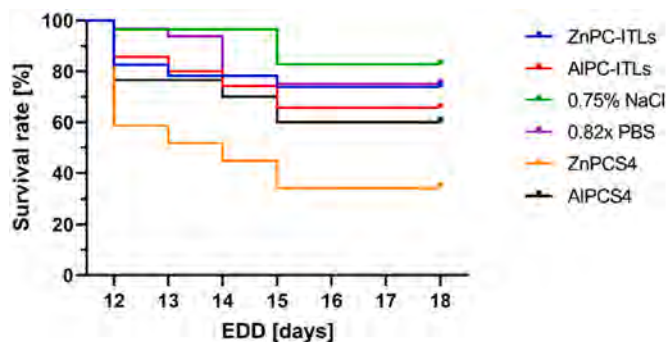


Fig. 9. Systemic toxicity in chicken embryos. Kaplan-Meier plot of chicken embryos that had received a single bolus of 1.2 nmol ZnPC and ALPC in ITLs and 128 nmol of ZnPCS4 and ALPCS4, accounting for a systemic PS concentration of 0.8 μM and 85 μM , respectively, in a 50- μL injection volume. Control group injections consisted of 0.75% NaCl solution and 0.82 \times PBS. Data encompass duplicate experiments with $N \geq 10$ /group.



Fig. 10. Clinical phototoxicity cases in non-resectable hilar cholangiocarcinoma patients who had undergone PDT with intravenously administered Photofrin (porfimer sodium) or Foscan (mTHPC) as a last-line treatment (palliative) of hilar cholangiocarcinoma. Phototoxicity was most prominent in regions most susceptible to light exposure (i.e., extremities, head, and neck) as well as at the infusion site (typically the vena cubiti). (A) Photo of a hand made after healing of severe burns with blisters, 3 months after injection of Photofrin into the vena cubiti. (B) and (C) Skin lesions both 2 months after intravenous injection of mTHPC, which ultimately healed by scarring (not shown). (D) and (E) Patient before (D) and 3 months after Photofrin-PDT (E) following a visit to an amusement park. The patient was wearing light-protective clothing, including a hat, but still experienced a severe photoallergic reaction in the face as evidenced by the degree of swelling. All patients were included in a clinical trial that had been approved by the institutional review board of the Academic Medical Center (AMC), University of Amsterdam, and registered under trial number NCT01016002. The trial was discontinued after inclusion of 5 patients due to the severity of adverse events. Explicit written informed consent for the publication of the images in (D) and (E) was provided posthumously to MH by the patient's spouse. Images and clinical metadata were provided to MH by Dr. Erik Rauws (AMC, retired).

relevant wavelength range (Fig. S4) and intensity. Mouse ears are well-vascularized and translucent, and therefore an ideal tool for visual inspection of overt phototoxicity. Also, the anatomy allows for pertinent physiological and pharmacodynamic processes such as PS extravasation and perivascular accumulation. As can be seen in Fig. 11A, ITL-delivered ZnPC inflicted numerous burn-like and erythemic wounds, often at multiple sites per ear, in 5 of the 8 ears (63%). Such damage patterns were absent in the ears of animals that had received AIPC-ITLs. ZnPCS4 induced similar type of damage in 3 of the 8 ears (38%), with one ear bearing a sizeable eschar. This was somewhat surprising given the photo-inactive character of ZnPCS4 reported above and in published work [20,21]. AIPCS4 was not associated with any apparent skin phototoxicity.

The most clear-cut histological sign of photochemical damage to the skin is the consequent immunological response; i.e., infiltration of the affected skin regions by inflammatory cells [107]. Accordingly, the degree of inflammatory cell influx was scored by histopathologists as described in the legend of Fig. 11. The scores are largely consistent with the macroscopic assessment, although the damage to ears induced by ZnPCS4 was not necessarily reflected in the histological appraisal. Control animals had a mean \pm SD score of 0.44 ± 0.53 , while mice subjected to AIPC-ITLs and AIPCS4 were scored as 0.33 ± 0.52 and 0.0 ± 0.0 , respectively. Skin sections of mice that were photosensitized with ITL-delivered ZnPC and ZnPCS4 were scored as 1.50 ± 0.53 and 0.25 ± 0.50 , respectively. The predominant site of inflammatory cell influx was the dermis (Fig. 11B-F), which is highly vascularized and allows immune cells to extravasate into photochemically afflicted zones along a chemotactic gradient [20,108].

It is not clear why ZnPC-ITLs caused significantly more skin phototoxicity than AIPC-ITLs. One possible explanation may be related to the relationship between particle diameter and the size of interendothelial junctions in the auricular microcirculation. The liposomal PS delivery systems were originally designed to prevent PS diffusion into skin as a result of the physical mismatch between the PEGylated liposomes and the endothelial fenestrations [20]. Although the ZnPC-ITLs and AIPC-ITLs had a mean diameter of 120 ± 8 nm and 175 ± 10 nm, respectively, that is larger than the 60-nm gaps between endothelial cells [109,110], particle sizes abide by a Gaussian distribution [21,23]. The smaller nanoparticle diameter shoulder may have overlapped with the larger size shoulder of the fenestration size histogram. Compared to the AIPC-ITLs, the smaller ZnPC-ITLs likely had a larger fraction of ITLs that could have passed through the fenestrations and accumulated in the perivascular space of mouse ears, causing more extensive damage

during the 24-h light exposure. Liposomal efflux from the microcirculation was observed with intravital fluorescence microscopy with NBD-labeled liposomes of similar composition and properties in hamster dorsal skin [111,112]. The same applied to the monovalent and tetravalent anionic fluorophores 5(6)-carboxyfluorescein and calcein, respectively, in intravital feasibility studies [111,112]. However, damage-based signs of intra-auricular accumulation of the tetrasulfonated PS derivatives, which are small charged molecules like 5(6)-carboxyfluorescein and calcein, were not observed. This dichotomy gives rise to another possible explanation, which is that ZnPC may have been extracted out of the phospholipid bilayer by a biomolecule such as low-density lipoprotein that facilitated the PS diffusion in a by proxy manner [20,21], as has been reported for non-PEGylated lecithin liposomes [113–115]. Whether PS extraction occurs with PEGylated liposomes and whether the phenomenon is more pronounced for ZnPC versus AIPC, which would add credence to the latter explanation, is currently being investigated.

3.8. ZnPC-ITLs and AIPC-ITLs Extend the Time to Sacrifice in a Mouse Model of Human Triple Negative Breast cancer

In the final set of pilot experiments, human triple-negative breast cancer (MDA-MB-231) cells were xenografted into BALB/c nude mice and left untreated (control) or subjected to PDT after photosensitization with ZnPC-ITLs and AIPC-ITLs (single bolus of 6 nmol PS, approximately 0.17 mg/kg body weight, 24-h dark-light interval). This tumor model was chosen because MDA-MB-231 xenografts are properly vascularized [116], which is necessary for optimal PS delivery [14,20], and because of precedent PDT studies [117–119], making benchmarking possible.

Mice did not respond adversely to the injection of PS or PDT as evidenced by comparable body weights relative to control animals (Fig. 12A). PDT resulted in smaller tumor volumes at every measurement point, with no pharmacodynamic potency difference between ZnPC and AIPC (Fig. 12B). PDT inflicted in the typical skin necrosis (dark patches) at the site of laser incidence (Fig. 12D) and caused a 4-day (33%) delay in the tumors reaching the human endpoint for both ZnPC-ITLs and AIPC-ITLs (Fig. 12C).

To get a general perspective of the PDT efficacy versus other PSs, the results were juxtaposed to results from other studies using the same xenograft model. Theodossiou et al. [119] used hypericin (12.5 mg/kg intraperitoneally, 2-h dark-light interval) to photosensitize tumors. PDT (cumulative radiant exposure of 40 J/cm^2 , Lumisource lamp with 530-nm long pass filter) resulted in a 14-day (47%) delay in the tumor

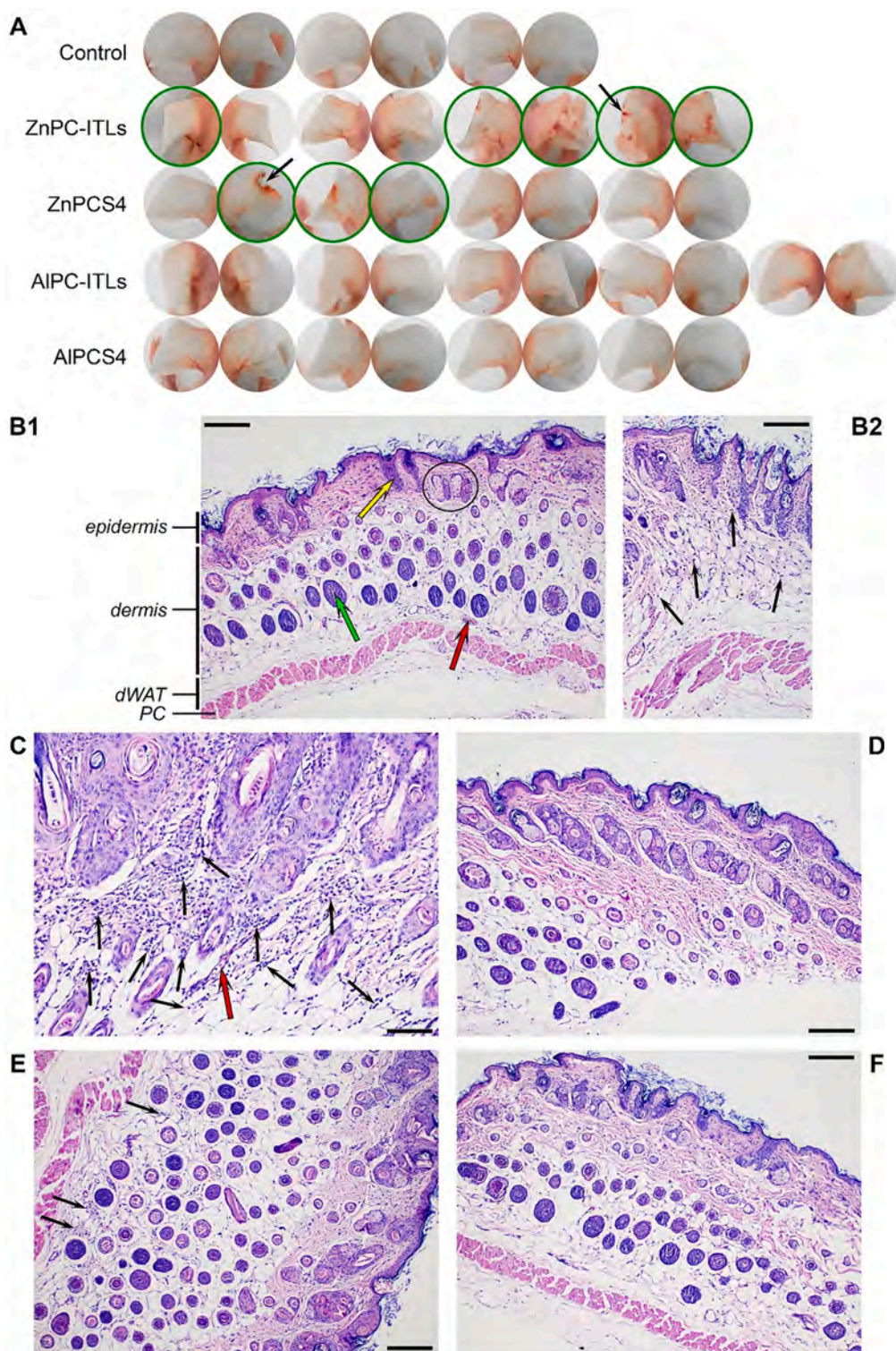


Fig. 11. PS phototoxicity in the ears and skin of nude mice. (A) Light-induced tissue injury in mouse ears 24 h after intravenous PS injection and continuous LED light exposure. The left and right ear of all animals included in the experiment were photographed and assessed for tissue injury resulting from PS activation by LED light (Fig. S4). Macroscopic tissue injury entailed visible burns characterized by eschars (ZnPCS4, arrow) and focal burn-like patches (ZnPC-ITLs, arrow). The panels depicting ears marked by photo-induced damage are outlined in green. Representative histology micrographs of dorsal skin of nude mice in the control group (not photosensitized; B1, B2) and animals that had received an intravenous bolus of ZnPC-ITLs (C), ZnPCS4 (D), AIPC-ITLs (E), and AIPCS4 (F). Legend for B1: green arrow, basis of a hair follicle; yellow arrow, hair follicle at the dermo-epidermal junction; red arrow, blood vessel; encircled, sebaceous glands surrounding two hair follicles. Abbreviations: dWAT, dermal white adipose tissue; PC, panniculus carnosus (muscle layer) [106]. The black arrows point to sites of inflammatory cell infiltrates as identified by the pathologist (TGK). Scale bar: 200 μ m (B1, D, E, F), 180 μ m (B2), 100 μ m (C). Histopathological scoring was performed as follows: 0, absence of inflammatory cell influx (e.g., D, F); 1, mild inflammatory cell influx (e.g., B2, E); 2, moderate inflammatory cell influx (e.g., C). (For interpretation of the references to color in this figure legend, the reader is referred to the web version of this article.)

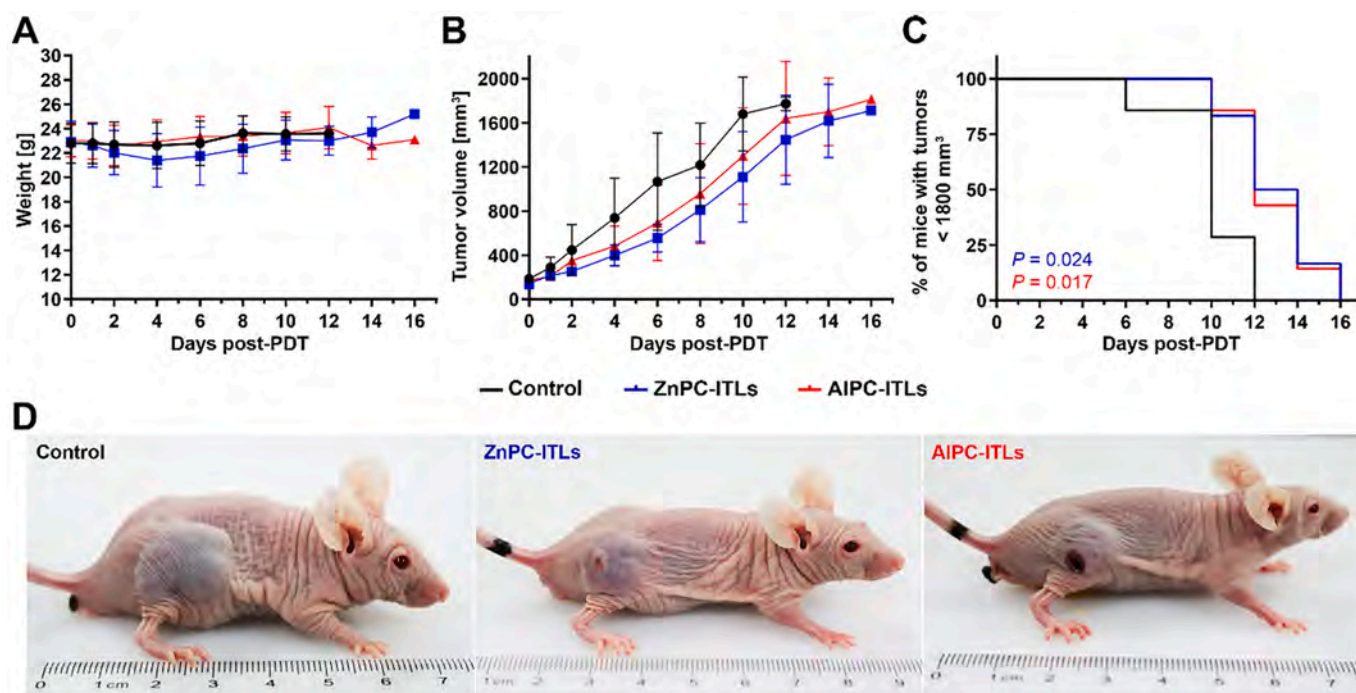


Fig. 12. PDT efficacy with ZnPC-ITLs and AIPC-ITLs in BALB/c nude mice bearing MDA-MB-231 xenografts. After reaching a tumor volume of 100–200 mm³ the animals were photosensitized with a single bolus of 6 nmol PS/animal and subjected to PDT (cumulative radiant exposure of 200 J/cm²) following a 24-h dark-light interval. Animal weights (A) were recorded and the tumor volume was measured and plotted as a function of time post-PDT (B). A Kaplan-Meier plot was constructed for the percentage of animals reaching a human endpoint (tumor volume of ≥ 1800 mm³) vs. time post-PDT (C). Data are plotted as mean \pm SD. Starting group size was $N = 6$ for ZnPC-ITLs and $N = 7$ for the control and AIPC-ITL group. Color-coded P -values are provided and are relative to the control group. Representative tumors are shown for mice on day 12 post-PDT (D).

volume reaching the predefined endpoint (≥ 1000 mm³). In the study by Wang et al. [118] BALB/c nude mice were photosensitized with 5-aminolevulinic acid (250 mg/kg intraperitoneally, 4-h dark-light interval) and subjected to PDT (cumulative radiant exposure of 120 J/cm², 400–700 nm filtered LED light). Extrapolation of the tumor volume-time curves yielded a 29% increase in the number of days (49 days in PDT group versus 38 days in control group) to reach an equivalent tumor volume, measured by fluorescence whole body imaging. Finally, Zhu et al. [117] photosensitized athymic nude mice with methyl pyropheophenylchlorin (15 mg/kg, 18-h dark-light interval) and performed PDT at a cumulative radiant exposure of 120 J/cm² using a 630-nm laser. Tumor volumes were plotted as a function of time after PDT, revealing a 46% reduction in tumor volume 23 d after PDT (data extrapolated from the graph). Our PDT efficacy results are therefore non-inferior to those obtained using other PSs from a tumor volume perspective and superior in light of the fact that the PS dose administered was at least 2 orders of magnitude lower than the dose used in the other studies.

The efficacy of the current modality could be optimized in several ways. Firstly, the PS:phospholipid molar ratio could be increased to augment the number of PS molecules delivered to a cell on a per liposome basis. A molar ratio of 0.003 has been used in all ITL studies conducted to date because this ratio was deemed optimal from a ROS production standpoint [23]. At higher ratios the ZnPC dimerizes or multimerizes [120], which results in photochemical deactivation and hampered biomolecule oxidation capacity [23]. However, ITLs should not be viewed as concrete ROS-generating entities in a tumor biological context. Liposomal constituents coalesce with cellular structures following ITL uptake (Fig. 2) and ZnPC and AIPC disperse homogeneously across the cellular environment (Fig. 4). As a result, liposomal PS dimerization/multimerization is of no concern due to dilution in the intracellular lipophilic compartment. ITLs with a PS:phospholipid molar ratio of 0.01 have been prepared before [23] and the ratio could be increased even further (unpublished results). Secondly, hybrid PS

delivery systems could be prepared encompassing e.g., AIPC in the lipid bilayer of liposomes and AIPCS4 in the lipid film hydration buffer, which would result in non-encapsulated as well as encapsulated AIPCS4 in the injectable bolus. If a high systemic presence of free AIPCS4 leads to any form of toxicity, the liposomes could be passed over a size exclusion chromatography column [121] to remove unencapsulated AIPCS4. The AIPCS4 would only be released from the liposome's aqueous compartment following ITL uptake or following an external stimulus, such as heat [111,121]. Thirdly, PSs other than AIPC or AIPCS4 can be loaded into the other platform components if warranted by preclinical research. A cocktail of PS-encapsulating ITLs, ETLS, and TTLs or permutations thereof could be administered as proposed earlier [20,21].

4. Conclusions

This study focused on the ITL component of the multi-component PS delivery platform designed to photosensitize the most relevant pharmacological target sites in a tumor: the tumor cells, the tumor vascular endothelium, and the tumor microenvironment including its cellular components. The ITLs encapsulating ZnPC and AIPC were further compared to their water-soluble tetrasulfonated counterparts in an array of rudimentary in vitro and in vivo experiments. The key findings were that [1] all PSs except for ZnPCS4 are able to effectively photosensitize cancer cells and non-cancerous cells, granted that the PSs actually reach the tumor environment after intravenous administration; [2] the pharmacodynamic potency of the photodynamically active PSs is considered highly toxic-to-potent as per anti-cancer compound classification; [3] the photodynamically active PSs do not elicit notable systemic toxicity in zebrafish and chicken embryos; [4] ITL-delivered ZnPC and ZnPCS4 are associated with skin phototoxicity, while the aluminum-containing PSs do not exert detectable skin phototoxicity; and [5] ITL-delivered ZnPC and AIPC are equally effective in their tumor-killing capacity in human tumor breast cancer xenografts and superior to other non-

phthalocyanine PSs when appraised on a per mole administered basis. The cutaneous phototoxicity of ZnPC(S4) in mice is worrisome. It is therefore concluded that AlPC(S4) are the least toxic and most effective and promising PSs to advance towards clinical translation using our comprehensive tumor targeting and PS delivery platform.

Author statement

Conceptualization – MJdK, ES, MHF, PMK, MH.
 Data curation – LMD, MJdK, DE, FS, DjdK, TGK, ED, JAK, LF, ACvW, EMS, MHF, ADB, YX, WP, MJdB, KCC, MH.
 Formal analysis – LMD, MJdK, DE, FS, TGK, ED, JAK, EMS, WP, VLT, PMK, MH.
 Funding acquisition – XH, SC, BD, MH.
 Investigation – LMD, MJdK, DE, FS, DjdK, TGK, ED, JAK, LPF, AcvW, EMS, MHF, ADB, MJdB, KCC, PMK, MH.
 Methodology – MJdK, DE, ED, JAK, EMS, MHF, WP, JB, RWS, VLT, SC, PMK, MH.
 Project administration – BD, PMK, MH.
 Resources – JEBC, XH, JB, RWS, VLT, SC, BD, PMK, MH.
 Supervision – LPF, MHF, JEBC, XH, WP, JB, RWS, VLT, SC, BD, PMK, MH.
 Validation – LMD, DjdK, TG, EMS, KCC.
 Visualization – LMD, MJdK, DE, FS, ED, JAK, LRdH, EMS, WP, VLT, PMK, MH.
 Writing - original draft – LMD, MJdK, DE, FS, DjdK, TGK, EMS, MHF, VLT, SC, PMK, MH.
 Writing - review & editing – LMD, MJdK, DE, JB, RWS, VLT, PMK, MH.

Declaration of Competing Interest

The authors declare that they have no known competing financial interests or personal relationships that could have appeared to influence the work reported in this paper.

Acknowledgements

This work was supported by grants from the Dutch Cancer Foundation (KWF project #10666), a Zhejiang Provincial Foreign Expert Program Grant, Zhejiang Provincial Key Natural Science Foundation of China (#Z20H160031), and a grant for the establishment of the Jiaying Key Laboratory for Photonanomedicine and Experimental Therapeutics to MH. BD is sponsored by grants from the National Natural Science Foundation (81872220), a Basic Public Welfare Research Project of Zhejiang Province (LGF18H160034), and the Tumor Nanotargeting and TCM Technology Innovation Team (Key Science and Technology Innovation Team of Jiaying, 2018). WP is sponsored by a grant from the National Natural Science Foundation of China (31871402). MH is chief formulation officer at Camelina Sun (whose business activities are unrelated to the present work).

The authors are grateful to Dr. Ruud Weijer for the BSA oxidation experiments and Dr. Marije Hoogland (pathologist at Isala, Zwolle, the Netherlands) for input on mouse histopathology.

Appendix A. Supplementary data

Supplementary data to this article can be found online at <https://doi.org/10.1016/j.jphotobiol.2022.112500>.

References

- [1] D.R. dos Santos Afda, L.F. Terra, M.S. Baptista, L. Labriola, Photodynamic therapy in cancer treatment - an update review, *J. Cancer Metastasis Treat.* 5 (25) (2019).
- [2] R. Weijer, S. Clavier, E.A. Zaal, M.M. Pijls, R.T. van Kooten, K. Vermaas, R. Leen, A. Jongejan, P.D. Moerland, A.H. van Kampen, et al., Multi-OMIC profiling of survival and metabolic signaling networks in cells subjected to photodynamic therapy, *Cell. Mol. Life Sci.* 74 (6) (2017) 1133–1151.
- [3] A.J. Sorrin, M. Kemal Ruhi, N.A. Ferlic, V. Karimnia, W.J. Polacheck, J.P. Celli, H. C. Huang, I. Rizvi, Photodynamic therapy and the biophysics of the tumor microenvironment, *Photochem. Photobiol.* 96 (2) (2020) 232–259.
- [4] M. Korbelik, Induction of tumor immunity by photodynamic therapy, *J. Clin. Laser Med. Surg.* 14 (5) (1996) 329–334.
- [5] M. Korbelik, J. Sun, I. Cecic, Photodynamic therapy-induced cell surface expression and release of heat shock proteins: relevance for tumor response, *Cancer Res.* 65 (3) (2005) 1018–1026.
- [6] R. Jayadevappa, S. Chhatre, H.J. Soukiasian, S. Murgu, Outcomes of patients with advanced non-small cell lung cancer and airway obstruction treated with photodynamic therapy and non-photodynamic therapy ablation modalities, *J. Thorac. Dis.* 11 (10) (2019) 4389–4399.
- [7] F.J. Bath-Hextall, R.N. Matin, D. Wilkinson, J. Leonardi-Bee, Interventions for cutaneous Bowen's disease, *Cochrane Database Syst. Rev.* 6 (2013), CD007281.
- [8] M.A. Gonzalez-Carmona, M. Bolch, C. Jansen, A. Vogt, M. Sampels, R.U. Mohr, K. van Beekum, R. Mahn, M. Praktijn, J. Nattermann, et al., Combined photodynamic therapy with systemic chemotherapy for unresectable cholangiocarcinoma, *Aliment. Pharmacol. Ther.* 49 (4) (2019) 437–447.
- [9] J.S. McCaughan Jr., E.C. Ellison, J.T. Guy, W.J. Hicks, J.J. Jones, L.R. Laufman, E. May, T.A. Nims, C.H. Spiridonidis, T.E. Williams, Photodynamic therapy for esophageal malignancy: a prospective twelve-year study, *Ann. Thorac. Surg.* 62 (4) (1996) 1005–1009 (discussion 9–10).
- [10] J. Lindenmann, V. Matzi, N. Neubeck, U. Anegg, E. Baumgartner, A. Maier, J. Smolle, F.M. Smolle-Juettner, Individualized, multimodal palliative treatment of inoperable esophageal cancer: clinical impact of photodynamic therapy resulting in prolonged survival, *Lasers Surg. Med.* 44 (3) (2012) 189–198.
- [11] H. Kostron, Photodynamic diagnosis and therapy and the brain, *Methods Mol. Biol.* 635 (2010) 261–280.
- [12] R. Baskaran, J. Lee, S.G. Yang, Clinical development of photodynamic agents and therapeutic applications, *Biomater Res.* 22 (2018) 25.
- [13] R. Weijer, M. Broekgaarden, R.F. van Golen, E. Bulle, E. Nieuwenhuis, A. Jongejan, P.D. Moerland, A.H. van Kampen, T.M. van Gulik, M. Heger, Low-power photodynamic therapy induces survival signaling in perihilar cholangiocarcinoma cells, *BMC Cancer* 15 (2015) 1014.
- [14] R. Weijer, M. Broekgaarden, M. Krekorian, L.K. Alles, A.C. van Wijk, C. Mackaaij, J. Verheij, A.C. van der Wal, T.M. van Gulik, G. Storm, et al., Inhibition of hypoxia inducible factor 1 and topoisomerase with acriflavine sensitizes perihilar cholangiocarcinomas to photodynamic therapy, *Oncotarget.* 7 (3) (2016) 3341–3356.
- [15] M. Broekgaarden, R. Weijer, M. Krekorian, B. van den Ijssel, M. Kos, L.K. Alles, A. C. van Wijk, Z. Bikadi, E. Hazai, T.M. van Gulik, et al., Inhibition of hypoxia-inducible factor 1 with acriflavine sensitizes hypoxic tumor cells to photodynamic therapy with zinc phthalocyanine-encapsulating cationic liposomes, *Nano Res.* 9 (6) (2016) 1639–1662.
- [16] M. Broekgaarden, R. Weijer, T.M. van Gulik, M.R. Hamblin, M. Heger, Tumor cell survival pathways activated by photodynamic therapy: a molecular basis for pharmacological inhibition strategies, *Cancer Metastasis Rev.* 34 (4) (2015) 643–690.
- [17] C.S. Shim, Y.K. Cheon, S.W. Cha, S. Bhandari, J.H. Moon, Y.D. Cho, Y.S. Kim, L. S. Lee, M.S. Lee, B.S. Kim, Prospective study of the effectiveness of percutaneous transhepatic photodynamic therapy for advanced bile duct cancer and the role of intraductal ultrasonography in response assessment, *Endoscopy.* 37 (5) (2005) 425–433.
- [18] R. Lindberg-Larsen, H. Solvsten, K. Kragballe, Evaluation of recurrence after photodynamic therapy with topical methylaminolevulinate for 157 basal cell carcinomas in 90 patients, *Acta Derm. Venereol.* 92 (2) (2012) 144–147.
- [19] S.L. Jacques, How tissue optics affect dosimetry of photodynamic therapy, *J. Biomed. Opt.* 15 (5) (2010), 051608.
- [20] R. Weijer, M. Broekgaarden, M. Kos, R. van Vught, E.A. Rauws, E.J. Breukink, T. M. van Gulik, G. Storm, M. Heger, Enhancing photodynamic therapy of refractory solid cancers: combining second-generation photosensitizers with multi-targeted liposomal delivery, *J. Photochem. Photobiol. C* 23 (2015) 103–131.
- [21] L.M. Dias, F. Sharifi, M.J. de Keijzer, B. Mesquita, E. Desclos, J.A. Kochan, D.J. de Klerk, D. Ernst, L.R. de Haan, L.P. Franchi, et al., Attritional evaluation of lipophilic and hydrophilic metallated phthalocyanines for oncological photodynamic therapy, *J. Photochem. Photobiol. B* 216 (2021), 112146.
- [22] M. Broekgaarden, R. van Vught, S. Oliveira, R.C. Roovers, P.M. van Bergen en Henegouwen, R.J. Pieters, T.M. Van Gulik, E. Breukink, M. Heger, Site-specific conjugation of single domain antibodies to liposomes enhances photosensitizer uptake and photodynamic therapy efficacy, *Nanoscale.* 8 (12) (2016) 6490–6494.
- [23] M. Broekgaarden, A.I. de Kroon, T.M. Gulik, M. Heger, Development and in vitro proof-of-concept of interstitially targeted zinc phthalocyanine liposomes for photodynamic therapy, *Curr. Med. Chem.* 21 (3) (2014) 377–391.
- [24] M. Broekgaarden, M. Kos, F.A. Jurg, A.A. van Beek, T.M. van Gulik, M. Heger, Inhibition of NF- κ B in tumor cells exacerbates immune cell activation following photodynamic therapy, *Int. J. Mol. Sci.* 16 (8) (2015) 19960–19977.
- [25] A.S. Derycke, P.A. de Witte, Liposomes for photodynamic therapy, *Adv. Drug Deliv. Rev.* 56 (1) (2004) 17–30.
- [26] G. Jori, Factors controlling the selectivity and efficiency of tumour damage in photodynamic therapy, *Lasers Med. Sci.* 5 (2) (1990) 115–120.
- [27] M. Broekgaarden, R. Weijer, A.C. van Wijk, R.C. Cox, M.R. Egmond, R. Hoebe, T. M. van Gulik, M. Heger, Photodynamic therapy with liposomal zinc phthalocyanine and tirapazamine increases tumor cell death via DNA damage, *J. Biomed. Nanotechnol.* 13 (2) (2017) 204–220.

- [28] Q. Peng, J.M. Nesland, Effects of photodynamic therapy on tumor stroma, *Ultrastruct. Pathol.* 28 (5–6) (2004) 333–340.
- [29] M.J. Bovis, J.H. Woodhams, M. Loizidou, D. Scheglmann, S.G. Bown, A. J. MacRobert, Improved in vivo delivery of m-THPC via pegylated liposomes for use in photodynamic therapy, *J. Control. Release* 157 (2) (2012) 196–205.
- [30] J. Buchholz, B. Kaser-Hotz, T. Khan, C. Rohrer Bley, K. Melzer, R.A. Schwendener, M. Roos, H. Walt, Optimizing photodynamic therapy: in vivo pharmacokinetics of liposomal meta-(tetrahydroxyphenyl)chlorin in feline squamous cell carcinoma, *Clin. Cancer Res.* 11 (20) (2005) 7538–7544.
- [31] O. Arrieta, L.A. Medina, E. Estrada-Lobato, L.A. Ramirez-Tirado, V.O. Mendoza-Garcia, J. de la Garza-Salazar, High liposomal doxorubicin tumour tissue distribution, as determined by radiopharmaceutical labelling with (99m)Tc-LD, is associated with the response and survival of patients with unresectable pleural mesothelioma treated with a combination of liposomal doxorubicin and cisplatin, *Cancer Chemother. Pharmacol.* 74 (1) (2014) 211–215.
- [32] D. Crivellari, K.P. Gray, S. Dellapasqua, F. Puglisi, K. Ribí, K.N. Price, I. Lang, L. Gianni, S. Spazzapan, G. Pinotti, et al., Adjuvant pegylated liposomal doxorubicin for older women with endocrine nonresponsive breast cancer who are NOT suitable for a "standard chemotherapy regimen": the CASA randomized trial, *Breast* 22 (2) (2013) 130–137.
- [33] A.Y. Bedikian, J.A. Silverman, N.E. Papadopoulos, K.B. Kim, A.E. Hagey, A. Vardeleon, W.J. Hwu, J. Homsí, M. Davies, P. Hwu, Pharmacokinetics and safety of Marqibo (vincristine sulfate liposomes injection) in cancer patients with impaired liver function, *J. Clin. Pharmacol.* 51 (8) (2011) 1205–1212.
- [34] M.A. Rodriguez, R. Pytlík, T. Kozák, M. Chhanabhai, R. Gascoyne, B. Lu, S. R. Deitcher, J.N. Winter, I. Marqibo, Vincristine sulfate liposomes injection (Marqibo) in heavily pretreated patients with refractory aggressive non-Hodgkin lymphoma: report of the pivotal phase 2 study, *Cancer* 115 (15) (2017) 3475–3482.
- [35] S. DiGiulio, FDA approves Onivyde combo regimen for advanced pancreatic cancer, *Oncol. Times* 37 (22) (2015) 8.
- [36] M.J. Reiniers, R.F. van Golen, S. Bonnet, M. Broekgaarden, T.M. van Gulik, M. R. Egmund, M. Heger, Preparation and practical applications of 2',7'-dichlorodihydrofluorescein in redox assays, *Anal. Chem.* 89 (7) (2017) 3853–3857.
- [37] K. Matsuo, F.G. Rocha, K. Ito, M.I. D'Angelica, P.J. Allen, Y. Fong, R.P. Dematteo, M. Gonen, I. Endo, W.R. Jarnagin, The Blumgart preoperative staging system for hilar cholangiocarcinoma: analysis of resectability and outcomes in 380 patients, *J. Am. Coll. Surg.* 215 (3) (2012) 343–355.
- [38] J. Valle, H. Wasan, D.H. Palmer, D. Cunningham, A. Anthoney, A. Maraveyas, S. Madhusudan, T. Iveson, S. Hughes, S.P. Pereira, et al., Cisplatin plus gemcitabine versus gemcitabine for biliary tract cancer, *N. Engl. J. Med.* 362 (14) (2010) 1273–1281.
- [39] T. Zoepf, R. Jakobs, J.C. Arnold, D. Apel, J.F. Riemann, Palliation of nonresectable bile duct cancer: improved survival after photodynamic therapy, *Am. J. Gastroenterol.* 100 (11) (2005) 2426–2430.
- [40] M. Wiedmann, F. Berr, I. Schiefke, H. Witzigmann, K. Kohlhaw, J. Mossner, K. Caca, Photodynamic therapy in patients with non-resectable hilar cholangiocarcinoma: 5-year follow-up of a prospective phase II study, *Gastrointest. Endosc.* 60 (1) (2004) 68–75.
- [41] M.E. Ortner, K. Caca, F. Berr, J. Lieberth, U. Mansmann, D. Huster, W. Voderholzer, G. Schachschal, J. Mossner, H. Lochs, Successful photodynamic therapy for nonresectable cholangiocarcinoma: a randomized prospective study, *Gastroenterology* 125 (5) (2003) 1355–1363.
- [42] F.L. Dumoulin, T. Gerhardt, S. Fuchs, C. Scheurle, M. Neubrand, G. Layer, T. Sauerbruch, Phase II study of photodynamic therapy and metal stent as palliative treatment for nonresectable hilar cholangiocarcinoma, *Gastrointest. Endosc.* 57 (7) (2003) 860–867.
- [43] A. Knuth, H. Gabbert, W. Dippold, O. Klein, W. Sachsse, D. Bitter-Suermann, W. Prellwitz, K.H. Meyer Zum Buschenfelde, Biliary adenocarcinoma. Characterisation of three new human tumor cell lines, *J. Hepatol.* 1 (6) (1985) 579–596.
- [44] M.F. Pansa, M.J. Lamberti, I.S. Cogno, S.G. Correa, N.B. Rumie Vittar, V. A. Rivarola, Contribution of resident and recruited macrophages to the photodynamic intervention of colorectal tumor microenvironment, *Tumour Biol.* 37 (1) (2016) 541–552.
- [45] C. Chuaysri, P. Thuwajit, A. Paupairoj, S. Chau-In, T. Suthiphongchai, C. Thuwajit, Alpha-smooth muscle actin-positive fibroblasts promote biliary cell proliferation and correlate with poor survival in cholangiocarcinoma, *Oncol. Rep.* 21 (4) (2009) 957–969.
- [46] G. Rouser, S. Fkeischer, A. Yamamoto, Two dimensional thin layer chromatographic separation of polar lipids and determination of phospholipids by phosphorus analysis of spots, *Lipids* 5 (5) (1970) 494–496.
- [47] I.C. Post, W.M. de Boon, M. Heger, A.C. van Wijk, J. Kroon, J.D. van Buul, T. M. van Gulik, Endothelial cell preservation at hypothermic to normothermic conditions using clinical and experimental organ preservation solutions, *Exp. Cell Res.* 319 (17) (2013) 2501–2513.
- [48] K.J. Harrington, G. Rowlinson-Busza, K.N. Syrigos, P.S. Uster, R.M. Abra, J. S. Stewart, Biodistribution and pharmacokinetics of ¹¹¹In-DTPA-labelled pegylated liposomes in a human tumour xenograft model: implications for novel targeting strategies, *Br. J. Cancer* 83 (2) (2000) 232–238.
- [49] M. Heger, I.I. Salles, W. van Vuure, I.H. Hamelers, A.I. de Kroon, H. Deckmyn, J. F. Beek, On the interaction of fluorophore-encapsulating PEGylated lecithin liposomes with hamster and human platelets, *Microwasc. Res.* 78 (1) (2009) 57–66.
- [50] M. Seshadri, J.A. Spornyak, R. Mazurchuk, S.H. Camacho, A.R. Oseroff, R. T. Cheney, D.A. Bellnier, Tumor vascular response to photodynamic therapy and the antivascular agent 5,6-dimethylxanthenone-4-acetic acid: implications for combination therapy, *Clin. Cancer Res.* 11 (11) (2005) 4241–4250.
- [51] W. Wang, L.T. Moriyama, V.S. Bagnato, Photodynamic therapy induced vascular damage: an overview of experimental PDT, *Laser Phys. Lett.* 10 (2) (2012), 023001.
- [52] J.V. Watson, S.H. Chambers, P.J. Smith, A pragmatic approach to the analysis of DNA histograms with a definable G1 peak, *Cytometry* 8 (1) (1987) 1–8.
- [53] D. Wlodkowic, J. Skommer, Z. Darzynkiewicz, Flow cytometry-based apoptosis detection, *Methods Mol. Biol.* 559 (2009) 19–32.
- [54] S.A. Hermens, E.J. van den Brandhof, L.T. van der Ven, A.H. Piersma, Relative embryotoxicity of two classes of chemicals in a modified zebrafish embryotoxicity test and comparison with their in vivo potencies, *Toxicol. in Vitro* 25 (3) (2011) 745–753.
- [55] K.C. Castricum, V.L. Thijssen, Method to study the role of galectins in angiogenesis in vivo using the chick chorioallantoic membrane assay, *Methods Mol. Biol.* (2022). In press.
- [56] A.E. Barnes, W.N. Jensen, Blood volume and red cell concentration in the normal chick embryo, *Am. J. Phys.* 197 (1959) 403–405.
- [57] R.F. van Golen, M.J. Reiniers, M. Heger, J. Verheij, Solutions to the discrepancies in the extent of liver damage following ischemia/reperfusion in standard mouse models, *J. Hepatol.* 62 (4) (2015) 975–977.
- [58] M.M. Jensen, J.T. Jorgensen, T. Binderup, A. Kjaer, Tumor volume in subcutaneous mouse xenografts measured by microCT is more accurate and reproducible than determined by ¹⁸F-FDG-microPET or external caliper, *BMC Med. Imaging* 8 (2008) 16.
- [59] H. Abrahamse, M.R. Hamblin, New photosensitizers for photodynamic therapy, *Biochem. J.* 473 (4) (2016) 347–364.
- [60] W.S. Chan, J.F. Marshall, R. Svendsen, J. Bedwell, I.R. Hart, Effect of sulfonation on the cell and tissue distribution of the photosensitizer aluminum phthalocyanine, *Cancer Res.* 50 (15) (1990) 4533–4538.
- [61] P. Qian, J.F. Evensen, C. Rimmington, J. Moan, A comparison of different photosensitizing dyes with respect to uptake C3H-tumors and tissues of mice, *Cancer Lett.* 36 (1) (1987) 1–10.
- [62] P. Cramers, M. Ruevekamp, H. Oppelaar, O. Dalesio, P. Baas, F.A. Stewart, Foscan uptake and tissue distribution in relation to photodynamic efficacy, *Br. J. Cancer* 88 (2) (2003) 283–290.
- [63] R.K. Jain, T. Stylianopoulos, Delivering nanomedicine to solid tumors, *Nat. Rev. Clin. Oncol.* 7 (11) (2010) 653–664.
- [64] S.C. Silverstein, R.M. Steinman, Z.A. Cohn, Endocytosis, *Annu. Rev. Biochem.* 46 (1977) 669–722.
- [65] W.A. Dunn, A.L. Hubbard, N.N. Aronson Jr., Low temperature selectively inhibits fusion between pinocytotic vesicles and lysosomes during heterophagy of 125I-asialofetuin by the perfused rat liver, *J. Biol. Chem.* 255 (12) (1980) 5971–5978.
- [66] G. Knoll, K.N. Burger, R. Bron, G. van Meer, A.J. Verkleij, Fusion of liposomes with the plasma membrane of epithelial cells: fate of incorporated lipids as followed by freeze fracture and autoradiography of plastic sections, *J. Cell Biol.* 107 (6 Pt 2) (1988) 2511–2521.
- [67] D. Montizaan, K. Yang, C. Reker-Smit, A. Salvati, Comparison of the uptake mechanisms of zwitterionic and negatively charged liposomes by HeLa cells, *Nanomedicine* 30 (2020), 102300.
- [68] J.S. Suk, Q. Xu, N. Kim, J. Hanes, L.M. Ensign, PEGylation as a strategy for improving nanoparticle-based drug and gene delivery, *Adv. Drug Deliv. Rev.* 99 (Pt A) (2016) 28–51.
- [69] Y. Sadzuka, K. Kishi, S. Hirota, T. Sonobe, Effect of poly(ethylene glycol) (PEG) chain on cell uptake of PEG-modified liposomes, *J. Liposome Res.* 13 (2) (2003) 157–172.
- [70] H. Hatakeyama, H. Akita, H. Harashima, The poly(ethylene glycol) dilemma: advantage and disadvantage of PEGylation of liposomes for systemic genes and nucleic acids delivery to tumors, *Biol. Pharm. Bull.* 36 (6) (2013) 892–899.
- [71] C.F. Buchanan, S.S. Verbridge, P.P. Vlachos, M.N. Rylander, Flow shear stress regulates endothelial barrier function and expression of angiogenic factors in a 3D microfluidic tumor vascular model, *Cell Adhes. Migr.* 8 (5) (2014) 517–524.
- [72] B.W. Engbrecht, C. Menon, A.V. Kachur, S.M. Hahn, D.L. Fraker, Photofrin-mediated photodynamic therapy induces vascular occlusion and apoptosis in a human sarcoma xenograft model, *Cancer Res.* 59 (17) (1999) 4334–4342.
- [73] E. Debeve, B. Pegaz, H. van den Bergh, G. Wagnieres, N. Lange, J.P. Ballini, Video monitoring of neovessel occlusion induced by photodynamic therapy with verteporfin (Visudyne), in the CAM model, *Angiogenesis* 11 (3) (2008) 235–243.
- [74] J.W. Yau, H. Teoh, S. Verma, Endothelial cell control of thrombosis, *BMC Cardiovasc. Disord.* 15 (2015) 130.
- [75] E. Hagtvet, T.J. Evjen, E.A. Nilssen, D.R. Olsen, Assessment of liposome biodistribution by non-invasive optical imaging: a feasibility study in tumour-bearing mice, *J. Nanosci. Nanotechnol.* 12 (3) (2012) 2912–2918.
- [76] G. Indrayanto, G.S. Putra, F. Suhud, in: A.A. Al-Majed (Ed.), Profiles of Drug Substances, Excipients and Related Methodology, Academic Press, 2021, pp. 273–307.
- [77] J.C. Pritchett, L. Naesens, J. Montoya, in: L. Flamand, I. Lautenschlager, G.R. F. Krueger, D.V. Abilash (Eds.), Human Herpesviruses HHV-6A, HHV-6B & HHV-7 (Third Edition), Elsevier, Boston, 2014, pp. 311–331.
- [78] A.P. Castano, T.N. Demidova, M.R. Hamblin, Mechanisms in photodynamic therapy: part one-photosensitizers, photochemistry and cellular localization, *Photodiagn. Photodyn. Ther.* 1 (4) (2004) 279–293.
- [79] O.A. Pena-Moran, M.L. Villarreal, L. Alvarez-Berber, A. Meneses-Acosta, V. Rodriguez-Lopez, Cytotoxicity, post-treatment recovery, and selectivity

- analysis of naturally occurring podophyllotoxins from *Bursera fagaroides* var. *fagaroides* on breast cancer cell lines, *Molecules*. 21 (8) (2016).
- [80] Y. Pan, Y. Yu, X. Wang, T. Zhang, Tumor-associated macrophages in tumor immunity, *Front. Immunol.* 11 (2020), 583084.
- [81] I. Beltran Hernandez, Y. Yu, F. Ossendorp, M. Korbelik, S. Oliveira, Preclinical and clinical evidence of immune responses triggered in oncologic photodynamic therapy: clinical recommendations, *J. Clin. Med.* 9 (2) (2020).
- [82] T. Soyama, A. Sakuragi, D. Oishi, Y. Kimura, H. Aoki, A. Nomoto, S. Yano, H. Nishie, H. Kataoka, M. Aoyama, Photodynamic therapy exploiting the anti-tumor activity of mannose-conjugated chlorin e6 reduced M2-like tumor-associated macrophages, *Transl. Oncol.* 14 (2) (2021), 101005.
- [83] M.V. Berridge, P.M. Herst, A.S. Tan, Tetrazolium dyes as tools in cell biology: new insights into their cellular reduction, *Biotechnol. Annu. Rev.* 11 (2005) 127–152.
- [84] H.L. Tang, H.M. Tang, K.H. Mak, S. Hu, S.S. Wang, K.M. Wong, C.S. Wong, H. Y. Wu, H.T. Law, K. Liu, et al., Cell survival, DNA damage, and oncogenic transformation after a transient and reversible apoptotic response, *Mol. Biol. Cell* 23 (12) (2012) 2240–2252.
- [85] H.M. Tang, H.L. Tang, Cell recovery by reversal of ferroptosis, *Biol. Open*. 8 (6) (2019).
- [86] Y.N. Gong, C. Guy, H. Olauson, J.U. Becker, M. Yang, P. Fitzgerald, A. Linkermann, D.R. Green, ESCRT-III acts downstream of MLKL to regulate necroptotic cell death and its consequences, *Cell*. 169 (2) (2017) 286–300 e16.
- [87] M. Overholtzer, J.S. Brugge, The cell biology of cell-in-cell structures, *Nat. Rev. Mol. Cell Biol.* 9 (10) (2008) 796–809.
- [88] O. Kepp, A. Marabelle, L. Zitvogel, G. Kroemer, Oncolysis without viruses - inducing systemic anticancer immune responses with local therapies, *Nat. Rev. Clin. Oncol.* 17 (1) (2020) 49–64.
- [89] H.S. Hwang, H. Shin, J. Han, K. Na, Combination of photodynamic therapy (PDT) and anti-tumor immunity in cancer therapy, *J. Pharm. Investig.* 48 (2) (2018) 143–151.
- [90] J. Zhou, G. Wang, Y. Chen, H. Wang, Y. Hua, Z. Cai, Immunogenic cell death in cancer therapy: present and emerging inducers, *J. Cell. Mol. Med.* 23 (8) (2019) 4854–4865.
- [91] X. Wang, Y. Lin, Tumor necrosis factor and cancer, buddies or foes? *Acta Pharmacol. Sin.* 29 (11) (2008) 1275–1288.
- [92] M. Wittayarath, A. Thongphakdee, K. Saikhun, K. Chatdarong, T. Otoi, M. Techakumpu, Cell cycle synchronization of skin fibroblast cells in four species of family Felidae, *Reprod. Domest. Anim.* 48 (2) (2013) 305–310.
- [93] A. Dalman, P. Eftekhari-Yazdi, M.R. Valojerdi, A. Shahverdi, H. Gourabi, E. Janzamin, R. Fakheri, F. Sadeghian, F. Hasani, Synchronizing cell cycle of goat fibroblasts by serum starvation causes apoptosis, *Reprod. Domest. Anim.* 45 (5) (2010) e46–e53.
- [94] P.K. Davis, A. Ho, S.F. Dowdy, Biological methods for cell-cycle synchronization of mammalian cells, *Biotechniques*. 30 (6) (2001) 1322 (-6, 8, 30-1).
- [95] J.S. Shin, S.W. Hong, S.L. Lee, T.H. Kim, I.C. Park, S.K. An, W.K. Lee, J.S. Lim, K. I. Kim, Y. Yang, et al., Serum starvation induces G1 arrest through suppression of Skp2-CDK2 and CDK4 in SK-OV-3 cells, *Int. J. Oncol.* 32 (2) (2008) 435–439.
- [96] Z. Jin, D.T. Dicker, W.S. El-Deiry, Enhanced sensitivity of G1 arrested human cancer cells suggests a novel therapeutic strategy using a combination of simvastatin and TRAIL, *Cell Cycle* 1 (1) (2002) 82–89.
- [97] E. Szliszka, Z.P. Czuba, A. Kawczyk-Krupka, K. Sieron-Stoltny, A. Sieron, W. Krol, Chlorin-based photodynamic therapy enhances the effect of tumor necrosis factor-related apoptosis-inducing ligand (TRAIL) in bladder cancer cells, *Med. Sci. Monit.* 18 (1) (2012) BR47–BR53.
- [98] D. Tudor, I. Nenu, G.A. Filip, D. Olteanu, M. Cenariu, F. Tabaran, R.M. Ion, L. Gligor, I. Baldea, Combined regimen of photodynamic therapy mediated by gallium phthalocyanine chloride and metformin enhances anti-melanoma efficacy, *PLoS One* 12 (3) (2017), e0173241.
- [99] V.H. Fingar, T.J. Wieman, P.S. Karavolos, K.W. Doak, R. Ouellet, J.E. van Lier, The effects of photodynamic therapy using differently substituted zinc phthalocyanines on vessel constriction, vessel leakage and tumor response, *Photochem. Photobiol.* 58 (2) (1993) 251–258.
- [100] Y. Huang, G. Xu, Y. Peng, H. Lin, X. Zheng, M. Xie, Zinc phthalocyanine tetrasulfonate (ZnPcS4): a new photosensitizer for photodynamic therapy in choroidal neovascularization, *J. Ocul. Pharmacol. Ther.* 23 (4) (2007) 377–386.
- [101] A. Viola, A. Jeunet, R. Decreau, M. Chanon, M. Julliard, ESR studies of a series of phthalocyanines. Mechanism of phototoxicity. Comparative quantitation of O2-. Using ESR spin-trapping and cytochrome c reduction techniques, *Free Radic. Res.* 28 (5) (1998) 517–532.
- [102] Y. Zhang, X. Chen, C. Gueydan, J. Han, Plasma membrane changes during programmed cell deaths, *Cell Res.* 28 (1) (2018) 9–21.
- [103] I.O.L. Bacellar, M.S. Baptista, Mechanisms of photosensitized lipid oxidation and membrane Permeabilization, *ACS Omega*. 4 (26) (2019) 21636–21646.
- [104] C. Cornet, S. Calzolari, R. Minana-Prieto, S. Dyballa, E. van Doornmalen, H. Rutjes, T. Savy, D. D'Amico, J. Terriente, ZeGlobalTox: an innovative approach to address organ drug toxicity using zebrafish, *Int. J. Mol. Sci.* 18 (4) (2017).
- [105] A. Vargas, M. Zeisser-Labouebe, N. Lange, R. Gurny, F. Delie, The chick embryo and its chorioallantoic membrane (CAM) for the in vivo evaluation of drug delivery systems, *Adv. Drug Deliv. Rev.* 59 (11) (2007) 1162–1176.
- [106] N. Naldaiz-Gastesi, O.A. Bahri, A. Lopez de Munain, K.J.A. McCullagh, A. Izeta, The panniculus carnosus muscle: an evolutionary enigma at the intersection of distinct research fields, *J. Anat.* (2018).
- [107] F. Fantini, A. Greco, A.M. Cesinaro, T. Surrenti, K. Peris, C. Vaschieri, A. Marconi, A. Giannetti, C. Pincelli, Pathologic changes after photodynamic therapy for basal cell carcinoma and Bowen disease: a histologic and immunohistochemical investigation, *Arch. Dermatol.* 144 (2) (2008) 186–194.
- [108] R. Falk-Mahapatra, S.O. Gollnick, Photodynamic therapy and immunity: an update, *Photochem. Photobiol.* 96 (3) (2020) 550–559.
- [109] H. Sarin, Physiologic upper limits of pore size of different blood capillary types and another perspective on the dual pore theory of microvascular permeability, *J. Angiogenesis. Res.* 2 (2010) 14.
- [110] S. Ono, G. Egawa, K. Kabashima, Regulation of blood vascular permeability in the skin, *Inflamm. Regen.* 37 (2017) 11.
- [111] M. Li, M.I. van Raath, S. Khakpour, A. Secilir, B.C. Sliggers, X. Huang, B. Ding, G. Storm, R.R. van der Hulst, A. de Kroon, et al., In vivo assessment of thermosensitive liposomes for the treatment of port wine stains by antifibrinolytic site-specific pharmacolaser therapy, *Pharmaceutics*. 12 (6) (2020).
- [112] M. Heger, I.I. Salles, R. Bezemer, M.A. Cloos, S.R. Mordon, S. Begu, H. Deckmyn, J.F. Beek, Laser-induced primary and secondary hemostasis dynamics and mechanisms in relation to selective photothermolysis of port wine stains, *J. Dermatol. Sci.* 63 (3) (2011) 139–147.
- [113] E. Reddi, C. Zhou, R. Biolo, E. Menegaldo, G. Jori, Liposome- or LDL-administered Zn (II)-phthalocyanine as a photodynamic agent for tumours. I. Pharmacokinetic properties and phototherapeutic efficiency, *Br. J. Cancer* 61 (3) (1990) 407–411.
- [114] B.A. Allison, P.H. Pritchard, J.G. Levy, Evidence for low-density lipoprotein receptor-mediated uptake of benzoporphyrin derivative, *Br. J. Cancer* 69 (5) (1994) 833–839.
- [115] L. Polo, G. Bianco, E. Reddi, G. Jori, The effect of different liposomal formulations on the interaction of Zn(II)-phthalocyanine with isolated low and high density lipoproteins, *Int. J. Biochem. Cell Biol.* 27 (12) (1995) 1249–1255.
- [116] R. Warin, D. Xiao, J.A. Arlotti, A. Bommarreddy, S.V. Singh, Inhibition of human breast cancer xenograft growth by cruciferous vegetable constituent benzyl isothiocyanate, *Mol. Carcinog.* 49 (5) (2010) 500–507.
- [117] J. Zhu, S. Tian, K.T. Li, Q. Chen, Y. Jiang, H.D. Lin, L.H. Yu, D.Q. Bai, Inhibition of breast cancer cell growth by methyl pyropheophenylchlorin photodynamic therapy is mediated through endoplasmic reticulum stress-induced autophagy in vitro and vivo, *Cancer Med.* 7 (5) (2018) 1908–1920.
- [118] X. Weng, D. Wei, Z. Yang, W. Pang, K. Pang, B. Gu, X. Wei, Photodynamic therapy reduces metastasis of breast cancer by minimizing circulating tumor cells, *Biomed. Opt. Express.* 12 (7) (2021) 3878–3886.
- [119] T.A. Theodossiou, M. Ali, M. Grigalavicius, B. Grallert, P. Dillard, K.O. Schink, C. E. Olsen, S. Walchli, E.M. Inderberg, A. Kubin, et al., Simultaneous defeat of MCF7 and MDA-MB-231 resistances by a hypericin PDT-tamoxifen hybrid therapy, *NPJ Breast Cancer.* 5 (2019) 13.
- [120] S.M. Nunes, F.S. Sguilla, A.C. Tedesco, Photophysical studies of zinc phthalocyanine and chloroaluminum phthalocyanine incorporated into liposomes in the presence of additives, *Braz. J. Med. Biol. Res.* 37 (2) (2004) 273–284.
- [121] M.I. van Raath, R. Weijer, G.H. Nguyen, B. Choi, A.I. de Kroon, M. Heger, Tranexamic acid-encapsulating thermosensitive liposomes for site-specific pharmacolaser therapy of port wine stains, *J. Biomed. Nanotechnol.* 12 (8) (2016) 1617–1640.